PNNL-24615
RPT-IGTP-005 Rev 0

Pacific Northwest
NATIONAL LABORATORY

Proudly Operated by Battelle Since 1965

Immobilized Low-Activity Waste Glass Release Data Package for the Integrated Disposal Facility Performance Assessment

VL Freedman
JV Ryan
DH Bacon

September 2015

U.S. DEPARTMENT OF ENERGY

Prepared for the U.S. Department of Energy
under Contract DE-AC05-76RL01830

DISCLAIMER

PACIFIC NORTHWEST NATIONAL LABORATORY
operated by
BATTELLE
for the
UNITED STATES DEPARTMENT OF ENERGY
under Contract DE-AC05-76RL01830

Printed in the United States of America

Available to DOE and DOE contractors from the
Office of Scientific and Technical Information,
P.O. Box 62, Oak Ridge, TN 37831-0062;
ph: (865) 576-8401
fax: (865) 576-5728
email: reports@adonis.osti.gov

Available to the public from the National Technical Information Service
5301 Shawnee Rd., Alexandria, VA 22312
ph: (800) 553-NTIS (6847)
email: orders@ntis.gov <http://www.ntis.gov/about/form.aspx>
Online ordering: http://www.ntis.gov

This document was printed on recycled paper.
(8/2010)

PNNL-24615
RPT-IGTP-005 Rev 0

Immobilized Low-Activity Waste Glass Release Data Package for the Integrated Disposal Facility Performance Assessment

VL Freedman
JV Ryan
DH Bacon

September 2015

Prepared for
the U.S. Department of Energy
under Contract DE-AC05-76RL01830

Pacific Northwest National Laboratory
Richland, Washington 99352

Executive Summary

The Hanford Site in southeastern Washington State has been used extensively by the U.S. Department of Energy (DOE) to produce nuclear materials for the U.S. defense arsenal. A large inventory of radioactive and mixed waste has accumulated in 177 buried single- and double-shell tanks. Liquid waste recovered from the tanks will be pretreated to separate the low-activity fraction from the high-level and transuranic wastes. The low-activity waste (LAW) is planned to be immobilized in glass, via vitrification, and placed into a near-surface disposal system on the Hanford Site. Before the immobilized low-activity waste (ILAW) can be placed into the disposal system, DOE must approve a performance assessment (PA), which documents the assumptions and provides the quantitative demonstration of compliance with the performance objectives for the long-term protection of the public and the environment. A critical component of the PA will be to demonstrate that releases from the selected glass waste form do not result in the performance objectives being exceeded. The PA must also, for purposes of establishing limits on radionuclides that may be buried near-surface, assess impacts to a hypothetical intruder and impacts to water resources.

The key information presented in this data package consists of the specific glass compositions and associated glass dissolution rate law parameters for five ILAW glasses. In addition, the results of geochemical modeling performed on several glasses that are not specifically described in this document are provided as supplemental data to help identify potential end-point alteration phases that may form during the weathering of ILAW glasses. These data (glass compositions, rate law parameters, and potential alteration phases) will be used to identify contaminant release source terms for the Integrated Disposal Facility PA. In addition, a general discussion on nuclear waste glass corrosion and a brief overview of modeling approaches and corresponding uncertainties are discussed.

Table ES.1 through Table ES.4 provide the specific data to be used to support the 2017 PA.

Table ES.1. Compositions (mass%) of ILAW Glasses to Support Waste Form Performance Assessments

Oxide	LD6-5412[(a)]	LAWABP1[(b)]	LAWA44[(c)]	LAWB45[(d)]	LAWC22[(d)]
Al_2O_3	12.00	10.00	6.20	6.13	6.08
B_2O_3	5.00	9.25	8.90	12.34	10.06
CaO	4.00	NI	1.99	6.63	5.12
Fe_2O_3	0.00	2.50	6.98	5.26	5.43
K_2O	1.46	2.20	0.50	0.26	0.10
La_2O_3	NI	2.00	NI	NI	NI
Li_2O	NI	NI	NI	4.62	2.51
MgO	NI	1.00	1.99	2.97	1.51
Na_2O	20.00	20.00	20.00	6.50	14.40
SiO_2	55.91	41.89	44.55	47.86	46.67
SO_3	0.21	0.10	0.10	0.84	0.34
TiO_2	NI	2.49	1.99	0.00	1.14
ZnO	NI	2.60	2.96	3.15	3.07
ZrO_2	NI	5.25	2.99	3.15	3.03
Others	1.42	0.72	0.85	0.29	0.54
Molecular Weight, g/mol[(e)]	63.99	69.11	66.96	62.41	64.31

(a) LD6-5412 – also known as HLP-46; see McGrail et al. (1998b) and Vienna et al. (2001).
(b) LAWABP1 – also known as HLP-51; see McGrail et al. (1999).
(c) LAWA44 – also known as HLP-56; see Muller et al. (2001).
(d) See Muller et al. (2001) for LAWB45 and LAWC22.
(e)Calculated as $MW_{glass} = \frac{\sum m_i}{\sum \left(m_i / MW_i \right)}$, where *i* represents each component in the complete composition (as noted in the references above), including components in "Others." Cationic species were assumed to be oxides in their most common oxidation state and anionic species were treated as elemental with no account for displaced oxygen.
NI = not included.
Others include minor amounts of Ag_2O, BaO, CdO, Ce_2O_3, Cl, Cr_2O_3, Cs_2O, F, I, MnO, MoO_3, Nd_2O_3, NiO, P_2O_5, PbO_2, Pr_2O_3, Re_2O_7, SeO_2, SrO, TeO_2, and Y_2O_3. Not all elements are present in every glass composition.

Table ES.2. Summary of Rate Law Parameters for 2017 PA Glasses at 15 °C

	Parameters							
	$\vec{k}_0$		K_g[(a)]	η	E_a	σ	r_{IEX}	
Glass	Reported Forward Rate Constant (g/[m^2 d])	Converted[(b)] Forward Rate Constant (mol/[m^2 s])	Glass Apparent Equilibrium Constant Based on Activity Product $a[SiO_2(aq)]$	pH Power Law Coefficient	Glass Dissolution Activation Energy (kJ/mol)	Temkin Coefficient	Na Ion-Exchange Rate (mol/[m^2 s])	Reference
LD6-5412	9.7×10^{6}	1.8×10^{0}	1.14×10^{-4}	0.40 ±0.03	74.8 ±1.0	1	1.74×10^{-11}[(c)]	McGrail et al. (1997)
LAWABP1	3.4×10^{6}	5.7×10^{-1}	4.90×10^{-4}	0.35 ±0.03	68 ±3.0	1	3.4×10^{-11}	McGrail et al. (2001a)
LAWA44	1.3×10^{4} ($R^2 = 0.78$)	2.2×10^{-3}	1.87×10^{-3} ($R^2 = 0.95$)	0.49 ±0.08	60 ±7	1	5.3×10^{-11}	Pierce et al. (2004)
LAWB45	1.6×10^{4} ($R^2 = 0.90$)	3.0×10^{-3}	1.79×10^{-3} ($R^2 = 0.78$)	0.34 ±0.03	53 ±3	1	0.0×10^{0}[(d)]	Pierce et al. (2004)
LAWC22	1.0×10^{5} ($R^2 = 0.98$)	1.8×10^{-2}	1.80×10^{-3} ($R^2 = 0.94$)	0.42 ±0.02	64 ±2	1	1.2×10^{-10}	Pierce et al. (2004)

(a) The K_g value for LD6-5412 is from McGrail et al. (1997), which states that value for chalcedony should be used; value given is K_g at 15 °C for chalcedony from the Geochemist's Workbench database thermo.com.V8.R6+.dat (Aqueous Solutions LLC 2015). The K_g values for LAWA44, LAWB45, and LAWC22 listed in this report are different from the values listed in Pierce et al. 2004, which were subject to a calculation error as pointed out in Papathanassiu et al. (2011). The error was associated with the use of the molecular weight for H_4SiO_4 (96.11 g/mol) instead of the molecular weight for Si (28.09 g/mol) during the calculation of the Si activity, which resulted in a factor of ~3.422 miscalculation. The erroneous K_g values for LAWA44, LAWB45, and LAWC22 were also reported in Pierce et al. (2010a, 2011, 2013) and Bacon and Pierce (2010). The K_g values for LD6-5412 and LAWABP1 were reported accurately in their source documents.

(b) The converted forward rate constant (mol/[m^2 s]) is calculated from the reported forward rate constant (g/[m^2 d]) divided by molecular weight of the given glass from Table ES.1 and converting time from days to seconds.

(c) Ion exchange rate for LD6-5412 is reported in Mann et al. (2001).

(d) No detectable ion exchange rate for LAWB45.

Table ES.3. Principal Alteration Phase Log K Values at 15 °C (Pierce et al. 2011)

Phase	Reaction	Log K (15 °C)
Analcime [$Na_{0.96}Al_{0.96}Si_{2.04}O_6 \bullet H_2O$]	Analcime + $3.84H^+ \leftrightarrow 0.96Al^{3+} + 0.96Na^+ + 2.04SiO_2(aq) + 2.92H_2O$	6.55
Anatase [TiO_2]	$TiO_2 + 2H_2O \leftrightarrow Ti(OH)_4(aq)$	-6.56
Baddeleyite [ZrO_2]	$ZrO_2 + 2H^+ \leftrightarrow Zr(OH)_2^{2+}$	-5.50
Calcite [$CaCO_3$]	$CaCO_3 + H^+ \leftrightarrow Ca^{2+} + HCO_3^-$	2.00
Chalcedony [SiO_2]	$SiO_2 \leftrightarrow SiO_2(aq)$	-3.64
$Fe(OH)_3(s)$	$Fe(OH)_3(am) + 3H^+ \leftrightarrow Fe^{3+} + 3H_2O$	6.16
Gibbsite [$Al(OH)_3$]	$Al(OH)_3 + 3H^+ \leftrightarrow Al^{3+} + 3H_2O$	8.37
Sepiolite [$Mg_4Si_6O_{15}(OH)_2 \bullet 6H_2O$]	Sepiolite + $8H^+ \leftrightarrow 4Mg^{2+} + 6SiO_2(aq) + 11H_2O$	46.27
$Zn(OH)_2$-γ	$Zn(OH)_2$-γ + $2H^+ \leftrightarrow Zn^{2+} + 2H_2O$	11.88

Table ES.4. Additional Alteration Phases

Phase	XRD Samples	SEM/EDS Samples
Gobbinsite [$Na_5(Si_{11}Al_5)O_{32} \bullet 11H_2O$]	2	---
Stevensite [$(Ca,Na)_xMg_{3-x}Si_4O_{10}(OH)_2$]	7	Possible
Hectorite-15a [$Na_{0.2}(Mg,Li)_3Si_4O_{10}(OH)_2 \bullet 4H_2O$]	1	---
Phillipsite-Na [$Na_4KAl_5Si_{11}O_{32}(H_2O)_{10}$]	1	Possible
Chabazite $Ca_2Al_4Si_8O_{24} \bullet 12H_2O$]	3	10
Herschelite [$NaAlSi_2O_6 \bullet 3H_2O$]	2	---
Saponite-15Å [$Ca_{0.2}Mg_3(SiAl)_4O_{10}(OH)_2 \bullet 4H_2O$]	1	Possible
Swinfordite-13Å [$Ca_{0.1}(Li,Al)_3Si_4O_{10}(OH)_2 \bullet 2H_2O$]	3	---
Foshagite [$Ca_4(SiO_3)_3(OH)_2$]	1	Possible
Iron Hydroxide [$Fe(OH)_3$]	---	Possible
Zinc Hydroxide [$Zn(OH)_2$]	---	Possible
Zirconium Hydroxide [$Zr(OH)_4$]	---	Possible

Acronyms and Abbreviations

aq	aqueous
AREST-CT	Analyzer for RadionuclidE Source-Term with Chemical Transport
ASME	American Society of Mechanical Engineers
ASTM	ASTM International, Standards Development Organization (www.astm.org)
BNFL	British Nuclear Fuels Limited
CHG	CH2MHill Hanford Group
DOE	U.S. Department of Energy
EDS	energy dispersive spectroscopy
eSTOMP	extreme-scale Subsurface Transport Over Multiple Phases (parallel computing version of computer model designated by "e")
FY	fiscal year
HLP	Hanford Low-Activity Waste Product
HLW	high-level waste
IDF	Integrated Disposal Facility
ILAW	immobilized low-activity waste
LAW	low-activity waste
NQA-1	ASME Nuclear Quality Assurance
PA	performance assessment
PCT	product consistency test
PCT-B	product consistency test method B
pH(T)	pH as a function of temperature
PNNL	Pacific Northwest National Laboratory
PRI	passivating reactive interphase
PUF	Pressurized Unsaturated Flow
QA	quality assurance
R&D	research and development
r_{IEX}	ion exchange rate
RFP	request for proposal
SCP	Software Control Package
SEM	scanning electron microscopy
SPFT	single-pass flow-through test
STOMP	Subsurface Transport Over Multiple Phases (serial version of computer model)
STORM	Subsurface Transport Over Reactive Multiphases (computer code)
TST	transition state theory
TWRS	Tank Waste Remediation System
TWRS-P	Tank Waste Remediation System-Privatization
VHT	Vapor Hydration Test
VSL	Vitreous State Laboratory

WRPS	Washington River Protection Solutions
WTP	Hanford Tank Waste Treatment and Immobilization Plant
WWFTP	WRPS Waste Form Testing Program
XRD	X-ray diffraction

Units of Measure

Bq	becquerel
°C	temperature in degrees Celsius [T(°C) = T(K) – 273.15]
d	day
g	gram
K	kelvin
kJ	kilojoules
L	liter
m	meter
M	molarity, mole/Liter
mL	milliliter
mass%	mass percent
mm	millimeter
mol	mole
nm	nanometer
ppm	parts per million
s	second
wt%	weight percent

Contents

Figures

Tables

1.0 Introduction

Federal facilities at the Hanford Site in southeastern Washington State have been used extensively by the U.S. government to produce nuclear materials for the U.S. strategic defense arsenal. Currently, the Hanford Site is under the stewardship of the U.S. Department of Energy (DOE) Office of Environmental Management. A large inventory of radioactive mixed waste resulting from the production of nuclear materials has accumulated, including high-level mixed waste[1] stored in 177 underground single- and double-shell tanks located in the Central Plateau of the Hanford Site (Mann et al. 2001). The DOE Office of River Protection is proceeding with plans to immobilize and permanently dispose of the low-activity waste (LAW) fraction on site in a shallow subsurface disposal facility (the Integrated Disposal Facility [IDF]).

1.1 Overview: ILAW Glass Disposal at Hanford

Currently, DOE plans to dispose of the glasses made from nuclear waste stored in underground tanks at Hanford at two U.S. locations: 1) the immobilized low-activity waste (ILAW) glass will be stored on site at the IDF and 2) the immobilized high-level waste (HLW) glass will be placed into a federal geologic repository. The solid and liquid waste recovered from the tanks will be pretreated to separate the low-activity fraction from the high-level and transuranic waste fractions. The LAW and HLW fractions will be separately immobilized into vitrified matrices (i.e., borosilicate glasses). Currently, vitrifying the LAW is expected to generate over 1.6×10^5 m^3 of glass (Certa and Wells 2010). Once vitrified, the volume of ILAW at Hanford will be the largest in the DOE complex, with one of the largest inventories (approximately 9.8×10^{14} Bq total activity) of long-lived radionuclides—principally ^{99}Tc ($t_{1/2} = 2.1 \times 10^5$ years), ^{129}I ($t_{1/2} = 1.6 \times 10^7$ years), and U—planned for disposal in a low-level waste facility.

Before the ILAW can be disposed of, DOE must conduct a performance assessment (PA) for the IDF that estimates the facility's impacts on the long-term protection of the public and the environment. One of the inputs to the PA is an estimate of radionuclide release rates from the engineered portion of the disposal facility (source term). These estimates are expected to be based on chemical reactions that occur in the near field and, in the case of ILAW glass, are controlled by the dissolution of the vitrified matrix. Therefore, to provide credible estimates, DOE must demonstrate a sufficient understanding of the coupled physiochemical processes that control glass dissolution to confirm that release rates will result in compliance with performance objectives for the long-term protection of the public and the environment.

A cornerstone assumption for the approach to estimating the source term is that the glass matrix must dissolve for radionuclides to be released into the environment. The dissolution rate is a function of glass composition, temperature, pH, surface area of the glass exposed to the contacting solution, and the composition of the solution contacting the glass. The temperature of the IDF is a known constant, 15 °C. However, both the pH and the composition of the solution contacting the glass are variables that are affected by infiltration rate, reactions with other engineered materials, gas-water equilibria, secondary-phase precipitation, alkali-ion exchange, and dissolution of the glass itself. Consequently, glass dissolution rates vary both in time and as a function of position in the disposal system. There is no single

[1] High-level mixed waste consists of radionuclides mixed with highly corrosive components, organics, or heavy metals that are regulated under the Resource Conservation and Recovery Act.

physical constant, such as a "leach rate" or radionuclide release parameter, that can credibly estimate the release of radionuclides from the glass waste form in such a dynamic system.

It is important to be able to demonstrate a sufficient understanding of the factors that influence releases from glass waste forms to support a reasonable expectation that release rates will not result in exceeding the established performance objectives. A reactive-chemical transport-modeling framework addressing the effects of fluid flow and glass-water reactions on the chemistry of pore-water percolating through the disposal facility can provide information to help support that basis. The fluid chemistry is coupled with kinetic rate equations that describe the response of the glass dissolution rate to changes in liquid composition in the disposal facility or repository, all computed as functions of time and space. These kinetic rate equations assume that (1) the dependence of dissolution and precipitation rates on departure from equilibrium is based on arguments and assumptions of Transition State Theory (TST), and (2) the driving force for transforming unstable silicate materials into stable ones is governed principally by the magnitude of displacement from thermodynamic equilibrium.

1.2 Laboratory Testing

The major goals of the PA activity are to

- support the design of disposal facilities,
- provide the technical basis for the DOE to authorize construction of disposal facilities,
- obtain approval to dispose of immobilized low-activity Hanford tank waste in those facilities, and
- provide a technical basis for final closure of the disposal facilities.

A critical component of the PA will be to demonstrate that releases from the selected glass waste forms do not result in the performance objectives being exceeded. A fundamental understanding and description of the processes and computer models can be used to support assumptions that are made for the PA. Details on the recommended technical strategy for developing this source term have been published (McGrail et al. 1998a), reviewed by an international panel of nuclear waste glass experts (Grambow et al. 2000), and those recommendations worked into future versions (Neeway et al. 2014a). This 2015 ILAW glass waste form release data package was developed from a direct implementation of that technical strategy.

This data package documents the input data that can be used to support a description of the expected behavior and serve as input for reactive transport simulations to support future PAs.[1] The reactive transport code, such as STORM, STOMP, and eSTOMP[2], requires input of two general classifications of data: 1) multiphase flow and 2) reactive transport. Hydraulic properties for multiphase flow simulations have been identified in data packages for both the near- and far-field (Meyer and Serne 1999; Meyer et al. 2004; Rockhold et al. 2015). Experimentally derived input related to conducting geochemical analyses is defined within this data package. Geochemist's Workbench and EQ3/6 can also be used to simulate the geochemical reactions.

[1] This data package is a living document that will be updated as new information becomes available.
[2] STORM (Subsurface Transport Over Reactive Multiphases [computer code]); STOMP (Subsurface Transport Over Multiple Phases [serial version of computer model]); and eSTOMP (extreme-scale Subsurface Transport Over Multiple Phases [parallel computing version of computer model designated by "e"]).

Laboratory testing provides the majority of the key input data required to assess the long-term performance of ILAW glasses (Figure 1.1 and Table 1.1). Four principal experimental methods, called out by McGrail et al. (1998a) and Neeway et al. (2014a), have been used to identify glass corrosion rates, but only two of these methods are discussed in this data package because they are relevant to the data provided: the single-pass flow-through test (SPFT) (ASTM C1662-10) and the product consistency test (PCT) (ASTM C1285-14).[1]

The different test methods focus on different aspects of the glass corrosion process and their principal functions, and the data they provide for modeling are given in Table 1.1. See McGrail et al. (1998a) and Neeway et al. (2014a) for additional details regarding all four test methods, including pressurized unsaturated flow (PUF) and vapor hydration test (VHT), and their use in evaluating long-term nuclear waste glass performance.

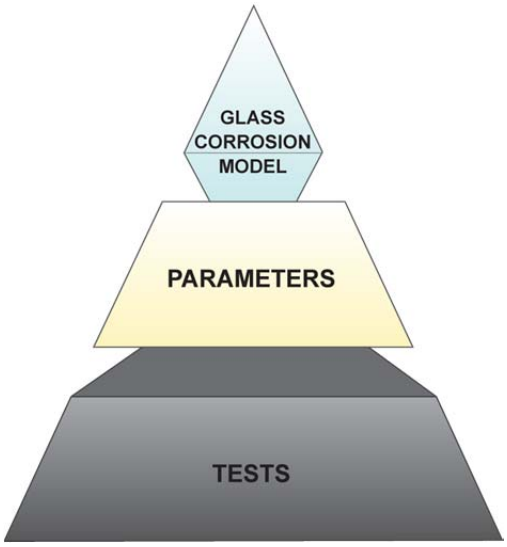

Figure 1.1. Schematic Diagram Showing that Experimental Tests Provide the Foundation for Parameter Estimates and the Parameters are the Basis for the Glass Corrosion Model

Table 1.1. Overview of Test Methods Discussed in this Data Package

Test Method	Temperature Range	Duration	Data Provided	Purpose
SPFT (ASTM C1662-10)	25° to 90 °C	14 to 28 days	Dissolution rate as a function of temperature, pH, and solution composition	Parameterization of kinetic rate law for glass dissolution
PCT (ASTM C1285-14)	20° to 100 °C	Weeks to years	Solution composition and dissolution rate as a function of surface area to volume ratio and temperature, secondary phases	Provide data for geochemical and reactive transport models

1.3 Report Purpose, Contents, and Organization

This report is meant to serve as a data package for specific glasses that will support the 2017 IDF PA. More specifically, this data package provides the glass compositions and rate law parameters for five ILAW glasses that either supported previous assessments or were formulated specifically for processing at the Hanford Tank Waste Treatment and Immobilization Plant (WTP). Additionally, the results of

[1] The pressurized unsaturated flow tests and vapor hydration test (ASTM C1663-09) are the other two test methods that can provide insight into glass corrosion rates or key alteration phases. It should also be noted that although ASTM C1285-14 is referenced, PCT data used in this data package may also have been developed under previous versions.

geochemical modeling performed on several glasses that are not specifically described in this document are provided as supplemental data to help identify potential end-point alteration phases that may form during the weathering of ILAW glasses. In addition to the specific PA data inputs, this report also provides a general discussion on nuclear waste glass corrosion and a brief overview of a geochemical modeling approach. While uncertainties with this approach exist, particularly in the applicability of secondary phases identified in static, 90 °C conditions to calculations performed in expected IDF conditions, the data in this work package represent the best data currently available. It is not within the scope of this document to provide a review of other potential modeling approaches or other experimental methods for obtaining data. However, limitations of methods are identified in the text to inform the reader, and external references are provided when appropriate.

1.4 Quality Assurance

This data package was funded by Washington River Protection Solutions (WRPS) under contract 36437-161, ILAW Glass Testing for Disposal at IDF. The work was conducted as part of Pacific Northwest National Laboratory (PNNL) Project 66309, ILAW Glass Testing for Disposal at IDF. The data presented in this document are data that have been compiled from previously published reports. No new data or conclusions are presented. Hence, the experimental and modeling results presented in this data package followed the QA practices implemented by those who generated and published the information.

Currently, all research and development (R&D) work at PNNL is performed in accordance with PNNL's laboratory-level Quality Management Program, which is based on a graded application of NQA-1-2000, *Quality Assurance Requirements for Nuclear Facility Applications*, to R&D activities. In addition to the PNNL-wide quality assurance (QA) controls, the QA controls of the WRPS Waste Form Testing Program (WWFTP) QA program were also implemented in preparing this report. The WWFTP QA program consists of the WWFTP Quality Assurance Plan (QA-WWFTP-001) and associated QA-NSLW-numbered procedures that provide detailed instructions for implementing NQA-1 requirements for R&D work. The WWFTP QA program is based on the requirements of NQA-1-2008, *Quality Assurance Requirements for Nuclear Facility Applications*, and NQA-1a-2009, *Addenda to ASME NQA-1-2008 Quality Assurance Requirements for Nuclear Facility Applications*, graded on the approach presented in NQA-1-2008, Part IV, Subpart 4.2, "Guidance on Graded Application of Quality Assurance (QA) for Nuclear-Related Research and Development". Preparation of this report was assigned the technology level "Applied Research" and was performed in accordance with procedure QA-NSLW-1102, *Scientific Investigation for Applied Research*. All staff members contributing to the preparation of the report have technical expertise in the subject matter and received QA training prior to performing quality-affecting work. The "Applied Research" technology level provides adequate controls to ensure that the compilation, review, and reporting activities were performed correctly. Use of both the PNNL-wide and WWFTP QA controls ensured that all client QA expectations were addressed in preparing this report.

2.0 Hanford ILAW Glass Performance Assessment

Over the past 19 years of testing and modeling, the LAW glass PA project has been focused on improving the technical defensibility of the PA for the disposal of ILAW glass at Hanford in accordance with the regulations in DOE Order 435.1-1 (DOE 1998), formerly DOE Order 5820.2A (DOE 1988). The first Hanford ILAW glass PA activity occurred shortly after the decision was made to change the ILAW form from grout to glass in the early 1990s. The major purpose of this initial activity, which was initiated under the Tank Waste Remediation System (TWRS) Immobilized Waste Program, was to evaluate design options for the engineered portion of the LAW disposal facility in preparation for an interim PA. This initial activity was completed in 1994 (Rawlins et al. 1994) and was revised in 1995 based on review comments and the incorporation of more accurate data (Mann 1995a).

Results from the initial evaluation illustrated that various performance parameters and key assumptions can significantly affect the design and the disposal facility's ability to achieve the required performance objectives. After the initial facility design evaluation, a data collection effort was initiated in an attempt to improve the technical basis for both the performance parameters and key conservative assumptions. The performance parameters and key assumptions included the radionuclide inventory, waste form release rates; and generic information for geologic data, geochemical data, hydraulic parameters, and water infiltration rates because the facility location and design were still in the planning stages. The generic geologic data, geochemical data, and hydraulic parameters, much of which originated from other DOE-sponsored projects and programs, were considered representative of the disposal area. The compiled information was documented in a series of data packages (Mann 1995a through 1995d; Mann et al. 1995) that were used as part of the 1996 interim PA (Mann et al. 1996; Mann 1997).

At this point in time, the privatization project (TWRS-P) request for proposal (RFP) (Wagoner 1996) was in the bidding process, and the composition of ILAW glass was not defined. Therefore, glass performance and subsequent radionuclide release rates in the 1996 interim PA base-case scenario used a constant leach rate that was based on a 20 °C, 7-day PCT limit as defined in the privatization project RFP (Mann et al. 1996). Because of a lack of information, it was assumed that the 7-day PCT response represented a conservative upper bound for glass performance and that short-term glass performance was representative of long-term behavior.

In addition to the base-case scenario, which used a constant release rate, sensitivity cases were conducted with a more mechanistic approach to modeling glass performance and radionuclide release using a numerical simulator, the AREST-CT (Analyzer for RadionuclidE Source-Term with Chemical Transport) computer code (Chen et al. 1995, 1997). As an alternative to a constant leach rate, the AREST-CT computer code allowed the chemical environment resulting from the glass dissolution reaction to be computed as a function of time and space in the disposal system. These sensitivity analysis results illustrated that the ^{99}Tc inventory and glass performance significantly affected radionuclide release estimates. The 1996 interim PA (Mann et al. 1996; Mann 1997) concluded that the preliminary and final PA would benefit from knowledge of the waste form, disposal facility location, and the disposal facility design as well as from extensive data collection for the generation of site-specific estimates for geologic data, geochemical data, hydraulic parameters, and water infiltration rates.

The PA conducted in 1998 was to support the application for a Disposal Authorization Statement (Mann et al. 1998) and coincided with a revision to the Radioactive Waste Management Order, which

changed from DOE Order 5820.2A (DOE 1988) to DOE Order 435.1 (DOE 1998). Before the data collection effort was initiated, an ILAW testing strategy was developed to guide the anticipated laboratory and field-scale testing and the model development activities to support future LAW glass in the disposal facility PAs at Hanford (McGrail et al. 1998a). The strategy was reviewed by a panel of national and international glass corrosion experts before being adopted by the TWRS program for the 1998 PA (Grambow et al. 2000; DOE 1999, 2001).

A major component of the testing strategy was the development of a numerical model that can compute time and spatial variations in the chemical environment of the unsaturated disposal systems in response to the corrosion of the glass waste forms as well as other physical and chemical processes. Development of the numerical simulator began in 1998 (McGrail and Bacon 1998; Mann 1997; Mann and Meyer 1998). Additionally, a set of experimental techniques that focused on different aspects of the glass corrosion process was outlined as part of the strategy. Collectively, these experimental techniques provided data needed to simulate long-term nuclear waste glass performance, based on the strategy outlined in McGrail et al. (1998a).

The numerical simulator approach was evaluated using rate parameter data collected from 1996 to 1997 on the LD6-5412 glass (composition provided in Table 2.1). The LD6-5412 glass was developed to serve as a simple reference glass during the TWRS privatization project (Wagoner 1996) for use in high-temperature melters with double-shell tank slurry feed supernatant waste composition (Mann et al. 1998; McGrail et al. 1997). The 1998 PA also used the 7-day PCT RFP limit as the base case; the rate law parameters derived from the LD6-5412 glass test data were used in sensitivity analyses using the AREST-CT computer code (Chen et al. 1995, 1997). The 1998 PA was substantially more robust than the previous iterations because of the increased understanding of waste form performance; disposal facility location; disposal facility design; and site-specific information on geologic data, geochemical data, hydraulic parameters, and water infiltration rates for the Central Plateau.

In support of the 2001 PA, scientists developed LAWABP1 (composition provided in Table 2.1) (McGrail et al. 2000a) to demonstrate that, with minor adjustments in composition, LAW glass with 20 wt% Na_2O could meet the DOE contract durability requirements, could demonstrate high performance in long-term corrosion testing, and would not exhibit accelerated corrosion (e.g., Stage III, see Section 3.0).

Similar to the data generated for LD6-5412, LAWABP1 was used as a representative LAW glass to generate model parameters (rate law parameters and identity of alteration phases) in support of the 2001 PA (Mann et al. 2001; McGrail et al. 2000a, 2001a). In addition to being documented in the 2001 PA, a journal article was published (McGrail et al. 2001b) to document the results of the experiments conducted on LAWABP1 and the STORM simulations used to forecast radionuclide release from the engineered portion of the disposal facility.

The Vitreous State Laboratory (VSL), subcontracted by Duratek Inc., British Nuclear Fuels Limited (BNFL), and CH2MHill Hanford Group (CHG), Inc., developed three reference glasses for LAW envelopes A, B, and C (i.e., LAWA44, LAWB45, and LAWC22, respectively) (Muller et al. 2001). These glasses met the new contract specifications (DOE 2000), have been processed using scaled joule heated melters, and are capable of being used to create ILAW in the WTP. The compositions of LAWA44, LAWB45, and LAWC22 are provided in Table 2.1. These three glasses were tested from 2001 to 2004, and the results were documented in the 2005 waste form release data package (Pierce et al.

2004) as well as a series of journal articles (Pierce et al. 2006, 2008a,b; Icenhower et al. 2002, 2004, 2008).

The reference glasses (LD6-5412 and LAWABP1) and the three envelope-based glasses (LAWA44, LAWB45, and LAWC22) are the focus of this data package. The glass compositions are provided in Table 2.1 while the rate law parameters and alteration phases needed to support the 2017 PA are provided in subsequent sections.

Table 2.1. Compositions (mass%) of ILAW Glasses to Support Waste Form Performance Assessments

Oxide	LD6-5412[(a)]	LAWABP1[(b)]	LAWA44[(c)]	LAWB45[(d)]	LAWC22[(d)]
Al_2O_3	12.00	10.00	6.20	6.13	6.08
B_2O_3	5.00	9.25	8.90	12.34	10.06
CaO	4.00	NI	1.99	6.63	5.12
Fe_2O_3	0.00	2.50	6.98	5.26	5.43
K_2O	1.46	2.20	0.50	0.26	0.10
La_2O_3	NI	2.00	NI	NI	NI
Li_2O	NI	NI	NI	4.62	2.51
MgO	NI	1.00	1.99	2.97	1.51
Na_2O	20.00	20.00	20.00	6.50	14.40
SiO_2	55.91	41.89	44.55	47.86	46.67
SO_3	0.21	0.10	0.10	0.84	0.34
TiO_2	NI	2.49	1.99	0.00	1.14
ZnO	NI	2.60	2.96	3.15	3.07
ZrO_2	NI	5.25	2.99	3.15	3.03
Others	1.42	0.72	0.85	0.29	0.54
Molecular Weight, g/mol[(e)]	63.99	69.11	66.96	62.41	64.31

(a) LD6-5412 – also known as HLP-46; see McGrail et al. (1998b) and Vienna et al. (2001).
(b) LAWABP1 – also known as HLP-51; see McGrail et al. (1999).
(c) LAWA44 – also known as HLP-56; see Muller et al. (2001).
(d) See Muller et al. (2001) for LAWB45 and LAWC22.
(e) Calculated as $MW_{glass} = \frac{\sum m_i}{\sum \left(m_i / MW_i \right)}$, where *i* represents each component in the complete composition (as noted in the references above), including components in "Others." Cationic species were assumed to be oxides in their most common oxidation state and anionic species were treated as elemental with no account for displaced oxygen.

NI = not included.
Others include minor amounts of Ag_2O, BaO, CdO, Ce_2O_3, Cl, Cr_2O_3, Cs_2O, F, I, MnO, MoO_3, Nd_2O_3, NiO, P_2O_5, PbO_2, Pr_2O_3, Re_2O_7, SeO_2, SrO, TeO_2, and Y_2O_3. Not all elements are present in every glass composition.

3.0 Theoretical Considerations for Glass Dissolution

Over the past 45 years, a large amount of data on the glass-water interaction has been collected. Two recent review articles by Gin et al. (2013) and Vienna et al. (2013a) summarized the state of the science. As shown by static dissolution test results ranging in composition from commercial glass to ILAW to vitrified HLW glass (Mišíková et al. 2007; Papathanassiu et al. 2011; Ebert 2014), aluminoborosilicate glass dissolution in a non-refreshed solution can be divided into three regimes or stages (Figure 3.1) that occur as the reaction proceeds (e.g., Stage I, II, and III):

- Stage I - Initial rate, r_o
- Stage II - Residual rate, r_r
- Stage III - Possible alteration rate renewal, r_a

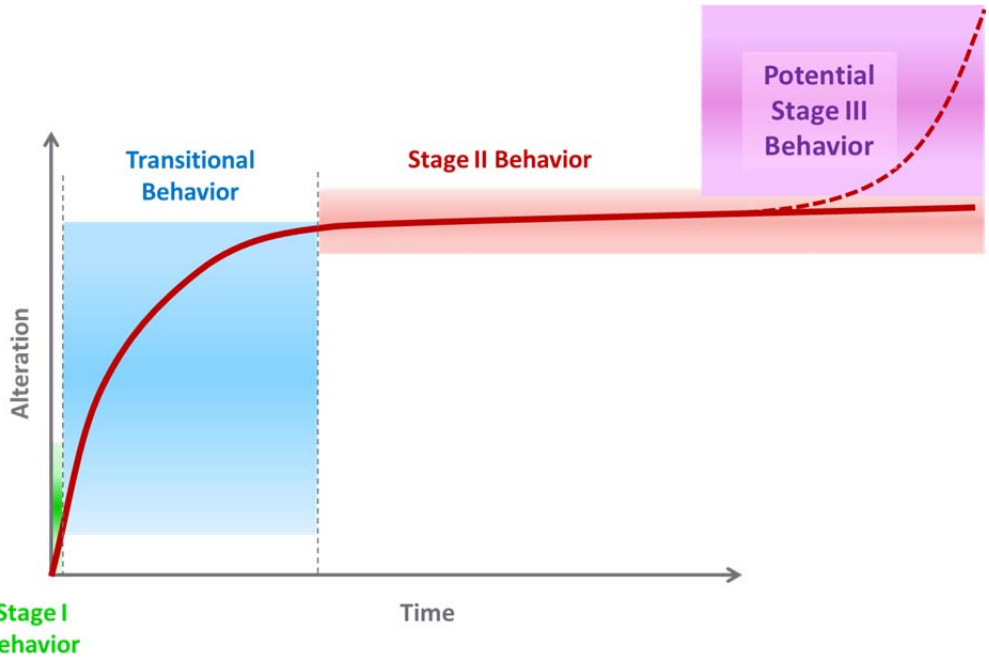

Figure 3.1. General Schematic of the Stages of Glass-Water Reaction

Briefly, Stage I represents the behavior of glass in an ideally dilute solution. In this case, hydrolysis occurs so rapidly that nearly all other mechanisms, with the possible exception of interdiffusion or ion exchange, are rendered irrelevant. Due to concentrations of key species already present in the groundwater (i.e. Q≠0; where Q is the ion activity product for glass), true Stage I behavior is not expected in the IDF repository. Under static conditions, increases in the ionic strength of the solution due to the dissolution of the glass accompany a decrease in the dissolution rate and the formation of a silica-rich amorphous hydrated surface layer (Bunker et al. 1983, 1986, 1988, 1994; Pederson et al. 1986). This decrease in dissolution rate can be modeled by a response to the chemical affinity of the system, which implicitly implies that the glass dissolution rate becomes dependent on the solution saturation state (concentration of elements in solution). This decrease in the rate of matrix dissolution is partially caused by the effect of silicic acid (H_4SiO_4 [aq]) on the dissolution rate and the formation of the hydrated surface

layer (Pierce et al. 2004, 2008a,b, 2010b; Icenhower et al. 2008; Abraitis et al. 2000). In other words, as the activity of H_4SiO_4 (aq) increases in the aqueous solution, the rate of glass dissolution decreases.

It is important to note that the dissolution rate, although low, does not become zero. The lowest observed rate of dissolution, the residual rate during Stage II behavior, is also not expected in the repository due to water infiltrating at low rates. Instead, the glass dissolution rate will be a function of the solution with which it is in contact. This solution, and more importantly, the activity of H_4SiO_4 (aq), is also affected by the formation of alteration phases in the alteration layers or the near field. These include clay minerals, such as a smectite or chlorite (Pierce et al. 2006, 2007). The precipitation kinetics associated with these phases can be complex, but in general, the rate of secondary phase growth increases in response to the increase in magnitude of supersaturation (Nagy and Lasage 1993; Nagy 1995).

Even as the glass dissolution slows and approaches Stage II, the process of interdiffusion or ion exchange, the selective removal of charge compensating cations (i.e., alkali and alkaline earth elements) by H^+ or H_3O^+, continues in accordance with a principle of interdiffusion into the solid undissolved glass. The release of ions from silicate glasses via ion exchange and hydrolysis has been well-documented (Casey and Bunker 1990; Bunker et al. 1983, 1986, 1988, 1994; Pederson et al. 1986). Ion exchange is a diffusive phenomenon, with release rates a function of the square root of time when the mechanism is isolated from other corrosion mechanisms (Neeway et al. 2014b). The conditions within the IDF, however, are not isolated. When dissolution is continually occurring, the rate of release due to diffusion in this coupled-mechanism state reaches a steady state, as can be experimentally shown (Feng and Pegg 1994a,b; McGrail et al. 2001c). Thus, for the ILAW glass dissolution model, ion exchange is modeled as a constant flux of sodium.

The altered layers (i.e., the interdiffusion zone, amorphous hydrated surface products [also known as the gel layer], and crystalline reaction products) represent a complex region, both physically and chemically, sandwiched between two distinct boundaries—pristine glass surface at the innermost interface and aqueous solution at the outermost interface. The thicknesses, chemical compositions, and pore structures of the altered layers change as a function of glass composition, pH, temperature, and bulk fluid composition. In addition, the altered layers are strongly affected by the formation of crystalline reaction products, whether in residual rate or alteration rate renewal regimes. Similar to nuclear waste glasses, altered layers have been identified on basaltic glasses (Casey and Bunker 1990; Wolff-Boenisch et al. 2004), mineral analogue glasses (Hamilton et al. 2001), medieval stained glasses (Sterpenich and Libourel 2006), and sodium borosilicate glasses (Geisler et al. 2010).

Acceleration of glass dissolution to a rate intermediate between Stage I and Stage II is sometimes seen in solutions with high ionic strength and is termed Stage III behavior. This behavior is correlated with the precipitation of secondary minerals that can significantly alter the composition of the fluid in contact with the glass. These phases, specifically zeolites, have been observed as precipitates, and it is hypothesized that their formation consumes key elements from solution (e.g., Al and Si) at a speed that is faster than the dissolution rate of the glass in the residual rate regime. Additionally, depending on the type of alteration phase, the glass-water reaction can cycle between the residual rate (i.e., Stage II) and alteration rate renewal (i.e., Stage III). This Stage III behavior has been observed in accelerated and long-term weathering experiments and may be associated with the Al/Fe ratio of the glass formulation (Jantzen et al. 2008). The rate acceleration is more likely with certain glass compositions (Ebert 2014; Ribet and Gin 2004), although most waste glass compositions will exhibit Stage III behavior under extreme experimental conditions (Gin and Mestre 2001). The triggers for Stage III behavior and the

propensity of various compositions to exhibit such behavior are poorly understood, particularly in the relatively low temperature conditions expected in the IDF. Additional research would be necessary to establish criteria to inform whether a particular composition/conditions set is likely to lead to Stage III behavior. However, nearly every observed instance of Stage III behavior occurred at 90 °C or higher. Due to the low temperature of IDF and the likelihood of solution refresh, Stage III behavior is thought to be much less likely in these conditions.

As a final note on the stages of glass dissolution, previous ILAW glass testing reports (Pierce et al. 2010a, 2011, 2013) split the generalized conceptual model for glass dissolution into five stages. In late 2013, the international nuclear waste glass corrosion community agreed to refer to the three stages described above rather than five (see Gin et al. 2013), and this approach is reflected in this report. The major difference is due to the recognition that none of the mechanisms that influence glass corrosion (dissolution, interdiffusion, reactive transport, and precipitation) can explain the long-term behavior alone. Thus, whereas several of the mechanisms were considered separately as interdiffusion (previously Stage I), hydrolysis (previously Stage II), and rate drop (previously Stage III), the evolution of these mechanisms is now recognized as a transition from Stage I (initial rate) to Stage II (residual rate) behavior under static conditions.

4.0 Kinetic Rate Law Parameters

4.1 Kinetic Rate Equation

A mathematical model that describes glass reactivity is needed to predict the long-term fate of glass in the subsurface over the period of regulatory concern. Glass-water interaction entails a complex set of coupled physicochemical mechanisms and a single equation or model that fully addresses the complexities and reflects observed behaviors has not yet been developed. Over the last few decades, a general rate equation based on arguments and assumptions of the TST has been developed to describe the dissolution of glass (and more ordered materials) in the presence of an aqueous solution. As described below, the equation is based upon the TST of chemical kinetics, in which the overall reaction rate is governed by the slowest elementary reaction. Elementary reactions have simple stoichiometry and can be combined as an overall reaction. In many cases, the elementary reactions can only be inferred. As an example of an elementary reaction, consider the dissolution of SiO_2 polymorphs to form silicic acid:

$$SiO_2(s) + 2H_2O \leftrightarrow SiO_2 \cdot 2H_2O^{\ddagger} \rightarrow H_4SiO_4(aq) \tag{4.1}$$

where $SiO_2 \bullet 2H_2O^{\ddagger}$ represents an activated complex. Note that a double-headed arrow, symbolizing a reversible reaction, links the reactants and the activated complex in Eq. (4.1). Equation (4.1) also illustrates that the TST formulation assumes that the decay of the activated complex is an irreversible reaction. Waste glasses represent a significantly more complex system, but the assumption is that a similar process, albeit largely unknown, defines their degradation. Due largely to these simplifications, this particular usage of the TST-based rate equation remains an active area of research. Although alternative conceptual models of glass dissolution include other controlling mechanisms such as reactive transport through an altered layer (Frugier et al. 2009) or a dissolution reprecipitation couple (Geisler et al. 2010; Hellman et al. 2015), each of these models (and others) includes a solution-affinity term in some form, pointing to a more general acceptance of the concept. A more complete discussion of the various approaches being investigated can be found in Neeway et al. (2014a) and Pierce et al. (2014). The conclusions of McGrail et al. (2000b) that the TST rate law best described the majority of experimental data collected over 35 years of glass/water reaction studies have not been successfully refuted to date. Therefore, the technical approach implemented for the 1998 and 2001 IDF PAs remains a robust strategy to modeling the key processes that control long-term ILAW glass corrosion, and this is a viable approach for the current iteration of the IDF PA.

Previous studies have established that the corrosion rate of silicate waste glasses depends strongly on temperature, pH, and the chemical composition of the aqueous solution contacting the glass (Cunnane et al. 1994a,b; Gin et al. 2013; Vienna et al. 2013a). When the aqueous solution is dilute, the glass dissolves at a characteristic forward rate that depends only on glass composition, temperature, and solution pH (McGrail et al. 1997, 2001b; Pierce et al. 2008a). In static systems, or where the rates of mass transport by fluid flow are slow, dissolution releases glass components into the aqueous solution, and the concentrations of these elements in the contacting fluid increase. The buildup of these dissolved components leads to slower glass corrosion rates as the contacting solution becomes more concentrated. As solution concentrations of dissolved elements continue to increase, solubility limits with respect to secondary phase(s) are reached, and these phases may begin to precipitate. A key factor controlling long-term durability of waste glasses is the rate of these processes.

The rate law that appears to best describe this overall dissolution behavior, developed by Aagaard and Helgeson (1982) and applied to glass by Grambow (1985), is presented as follows:

$$r_i = \overrightarrow{k_o} \nu_i a_{H^+}^{-\eta} \exp\left(\frac{-E_a}{RT}\right)\left[1 - \left(\frac{Q}{K_g}\right)^{\sigma}\right]\prod_j a_j \qquad (4.2)$$

where
r_i = dissolution rate, g m^{-2} d^{-1}
$\vec{k}_0$ = intrinsic rate constant, g m^{-2} d^{-1}
ν_i = mass fraction of component *i*, unitless
a_{H^+} = hydrogen ion activity
E_a = apparent activation energy, kJ/mol
R = gas constant, kJ/(mol·K)
T = temperature, K (assumed constant at 15 °C or 288 K)
Q = ion activity product for glass
K_g = pseudo-equilibrium constant
a_j = activity of *j*th species
η = pH power law coefficient
σ = Temkin coefficient (σ = 1 assumed).

The chief virtue of Eq. (4.2) is that it can be incorporated into reaction-transport codes to simulate the dissolution behavior of glass under specific storage conditions. Another benefit of Eq. (4.2) is that it is based on the TST of chemical kinetics, in which a series of reaction rates are governed by the slowest elementary reaction. Therefore, it is simply necessary to ascertain the rate-limiting step in dissolution rather than attempt to fully understand all of the possible reactions and kinetic pathways that can occur during the reaction of glass with aqueous solution. Because this rate-limiting step is an "elementary reaction," the stoichiometry of the reaction is typically simple and can be easily defined in a geochemical model.

In addition, test results with ILAW glasses show that these high-sodium-containing glasses are susceptible to a secondary reaction mechanism, alkali-ion exchange (Boksay et al. 1968; Doremus 1975). In this reaction, alkali in the glass are released into solution and replaced in the solid glass structure with an equimolar amount of a hydrogen-containing monovalent ion (H^+ or H_3O^+). The rate of this ion-exchange reaction, referred to hereafter as r_{IEX}, has been determined from SPFT for numerous glasses (McGrail et al. 2001a,b,c; Pierce et al. 2004; Papathanassiu et al. 2011). Although ion exchange is recognized as a diffusive phenomenon (with a resulting release rate as a function of the square root of time), in a system with continuous flow of infiltration water and continuous dissolution, the rate of release due to diffusion reaches a steady state. This is reflected in the near constant release rate routinely observed in tests with ILAW. For this reason, the constant values obtained in the above studies are used for the rate law.

4.2 Parameterization Results

The SPFT method (ASTM C1662-10) is the approach used to determine the kinetic rate law parameters presented in Eq. (4.2); k, E_a, η, and K_g. Briefly, SPFT is an open system test where an influent solution is pumped, at a known flow rate and constant temperature, through a reaction cell that contains the glass sample (Figure 4.1). The configuration precludes recirculation of the effluent and thus makes a single pass through the reaction cell. Although there are various designs of the SPFT system (i.e., well-mixed batch reactor, packed bed, and fluidized bed), all SPFT data discussed in this report were collected using the well-mixed batch reactor design.

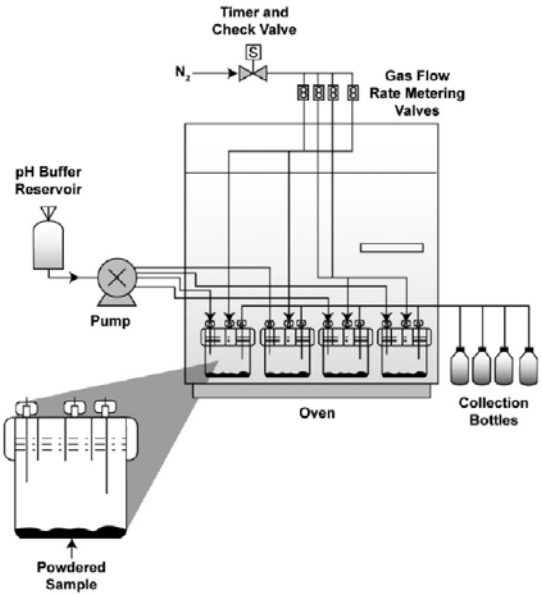

Figure 4.1. Schematic of the Single-Pass Flow-Through Test Method (well-mixed batch reactor design)

In brief, the SPFT apparatus consists of syringe pumps that transfer solution from input reservoirs to the reactors via Teflon tubing. The perfluoroalkoxy Teflon reactor (Savillex, Minnetonka, MN) consists of two pieces that thread together to form a cylinder with a total inner volume of ~80 mL. The relatively large diameter of the sample holder allows the glass particles to form a thin layer at the reactor bottom and interact largely independently with the contacting solution. The experimental system pumps a continuous flow of fresh influent solution, which 1) prevents the buildup of reaction products, 2) maintains the bulk solution composition throughout the duration of an experiment, 3) allows an investigator to directly quantify the dissolution rate, and 4) allows the reactivity of material to be studied over a wide range of experimental conditions. Therefore, by design, the SPFT experiment minimizes the accumulation of reaction products and the subsequent formation of an alteration layer. For a more detailed description of this method, see McGrail et al. (1997).

The following sections briefly summarize the kinetic rate law parameter results collected for LD6-5412, LAWABP1, LAWA44, LAWB45, and LAWC22 from SPFT testing.

4.2.1 LD6-5412 Glass Results

McGrail et al. (1997, 1998a) and Mann et al. (1998) document the results collected for LD6-5412. This section focuses on a subset of those results germane to this data package, specifically the kinetic rate law parameters. Two types of SPFT experiments were conducted. The first SPFT series varied the flow rate to sample surface area (q/S) and were used to determine chemical affinity parameters; whereas the second set was conducted under dilute conditions at a fixed flow rate and varied pH and temperature, and was used to determine k, E_a, and η. The q/S experiments were conducted at 40 °C and pH = 9.0 and were used to estimate the silica saturation value silica polymorph, C_{Si}^*, and a rate constant, k_o, for both aluminum and silicon. Here the values reported are derived from Si release, which were $C_{Si}^* = 3.18 \pm 0.08$ and $k_o = 1.19 \times 10^{-7} \pm 2.31 \times 10^{-9}$ g/(m^2 s).

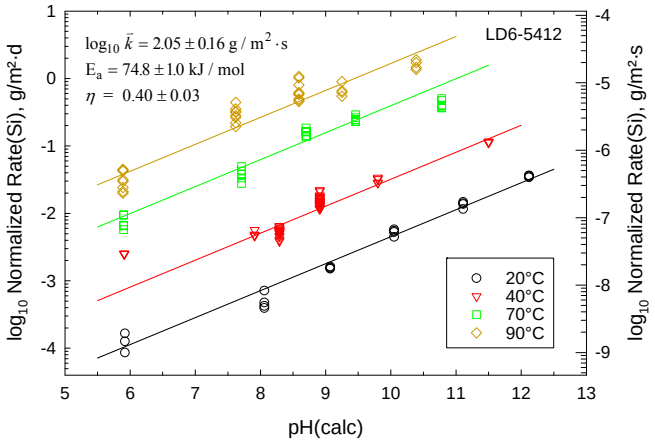

Figure 4.2. Normalized Silica Release Rate as a Function of pH and Rate Law Parameters for Reference Glass LD6-5412. The LD6-5412 Glass Was Developed during Part A of TWRS privatization project. (Graph from McGrail et al. 1998a.)

The experiments conducted under dilute conditions were performed as a function of temperature (20°, 40°, 70°, and 90 °C) and pH (pH[23 °C] = 6, 8, 9, 10, 11, and 12) to determine $\bar{k}$, E_a, and η. Prior to calculating rate law parameters, McGrail et al. (1997) used EQ3NR and the single-pass flow-through analyzer (SIPFT) code to estimate conditions that were saturated with respect to Ca, Al, and Si. This estimate was used to adjust the calculated rates for the effect of chemical affinity. It is important to note that McGrail et al. (1997) used H_3BO_3 as a pH buffer solution; therefore, B could not be used as a tracer for glass corrosion. Figure 4.2 shows the results of the normalized release rates based on Si, as a function of pH and temperature. A linear regression of the data at each temperature yielded the parameters shown in Table 4.1. These parameters were used in a sensitivity case in the 1998 PA for predicting LD6-5412 glass corrosion rates with the AREST-CT code (Mann et al. 1998).

4.2.2 LAWABP1 Glass Results

The kinetic rate law parameters for LAWABP1 were documented in McGrail et al. (2001a,b). Figure 4.3 illustrates the forward dissolution rate data for LAWABP1 glass as a function of temperature (23°, 40°, 70°, and 90 °C) and pH (pH[23 °C] = 7, 8, 9, 10, 11, and 12). It is important to note that buffer solutions used in these experiments were tris hydroxymethyl aminomethane for pH(23 °C) 7 to 10 and a mixture of LiOH/LiCl for pH(23 °C) 11 and 12. Because the design of the SPFT experiment maintains dilute conditions, the chemical affinity term $(1 - Q/K)$ in Eq. (4.2) can be neglected and a non-linear regression of the data at each temperature can be used to estimate the parameters ($\vec{k}$, η, E_a). The results of the linear regression yielded the parameters shown in Table 4.1.

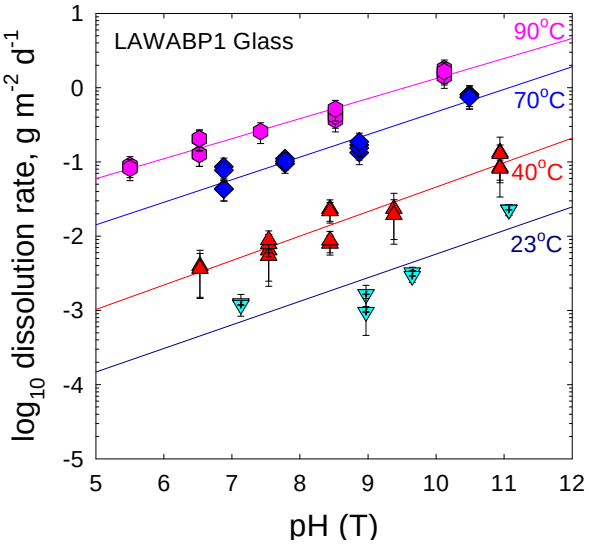

Figure 4.3. Normalized Glass Dissolution Rate, Based on Boron, as a Function of pH(T) for LAWABP1 (from McGrail et al. 2001a).

Along with the rate law parameters $\vec{k}$, η, E_a, the parameters K (in this case K_g where g represents the glass) and r_{IEX} were also determined for LAWABP1. This was accomplished by doping the inlet solution with silicon over concentration ranges based on the saturation value of amorphous silica at the various temperatures; generally 1 to 140 ppm Si. The results of this experiment are presented in Figure 4.4 where the dissolution rates with respect to boron and sodium are plotted as a function of the activity of silcic acid. It is seen that the glass dissolution rate decreases rapidly and then reaches a constant value with increasing activity of silicic acid. In order to derive a theoretical estimate for K_g, a linear regression is performed in the section of the diagram where the dissolution rate of the glass decreases with respect to the silicic acid activity. By performing the linear regression at the various temperatures, the K_g value for LAWABP1 can be estimated at 15 °C as demonstrated in Figure 4.5 where the K_g(15 °C) value is 4.90×10^{-4}.

In addition to the K_g value, the r_{IEX} value can also be determined from the data presented in Figure 4.4 where the dissolution rate measured from sodium is consistently greater than the dissolution rate measured from boron. The r_{IEX} value is computed by subtracting the steady-state sodium release rate from the steady-state matrix dissolution rate, indexed by boron, and converted to moles of sodium per square meter per second. By performing this calculation at the various experimental temperatures, the natural logarithm of r_{IEX} is plotted as a function of the inverse temperature in Kelvin, as presented in Figure 4.6. The value of r_{IEX} is then calculated at 15 °C, which was determined to be 5.3×10^{-11} mol m^{-2} s^{-1}.

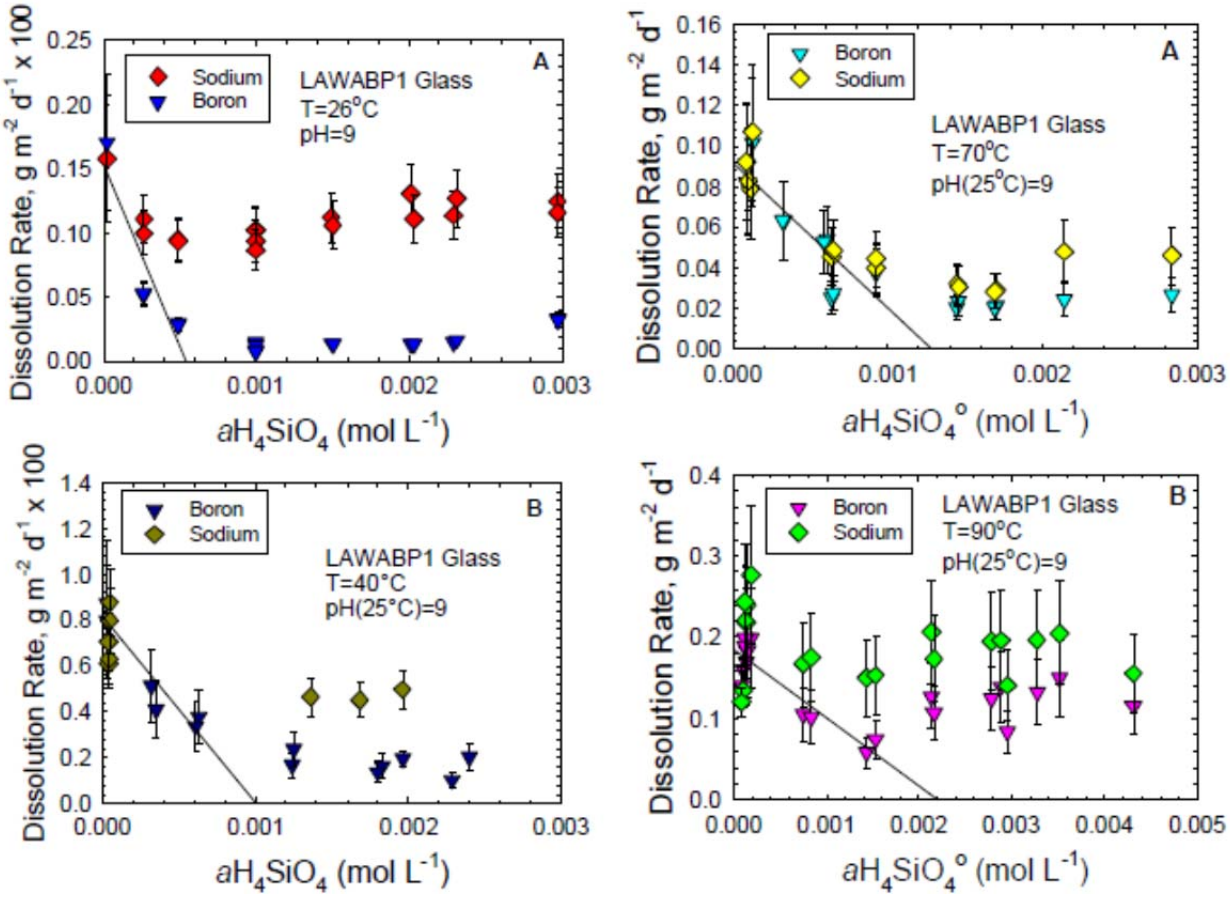

Figure 4.4. Plot of Dissolution Rate vs. the Activity of Silicic Acid for LAWABP1 Glass. (McGrail et al. 2001a)

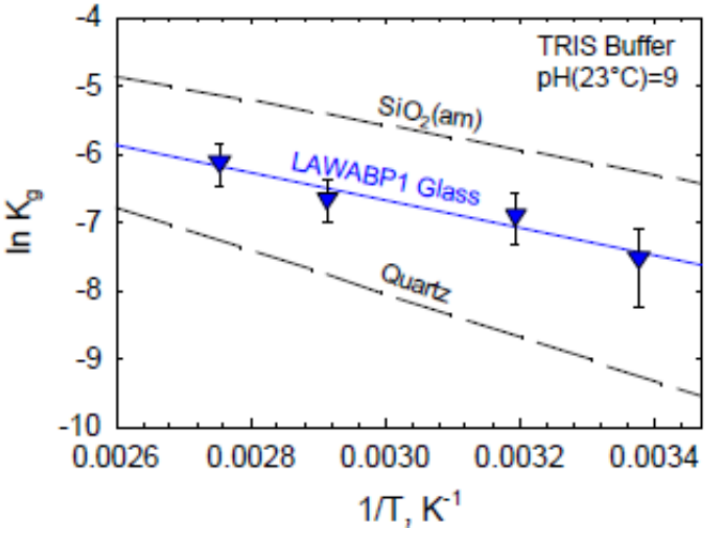

Figure 4.5. log Kg vs. 1/T for LAWABP1 Glass. (McGrail et al. 2001a)

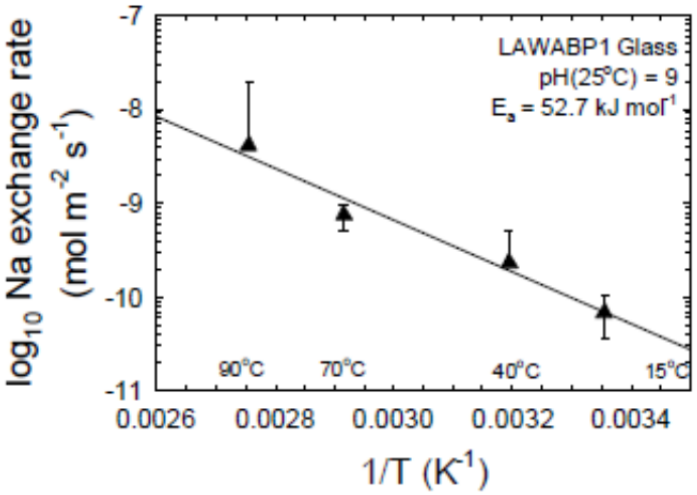

Figure 4.6. Sodium Ion Exchange Rate vs. Reciprocal Temperature for LAWABP1 Glass (McGrail et al. 2001a)

4.2.3 LAWA44, LAWB45, and LAWC22 Glass Results

From 2001 to 2004, three glass samples (LAWA44, LAWB45, and LAWC22) were evaluated in support of the 2005 ILAW PA calculations (Pierce et al. 2004). The composition for each glass is provided in Table 2.1. Each glass sample underwent SPFT experiments as a function of pH and temperature under dilute conditions and as a function of $a[SiO_2(aq)]$ and temperature from dilute to near-saturated conditions with respect to amorphous silica. Again, buffer solutions used in these experiments were tris hydroxymethyl aminomethane for pH(23 °C) 7 to 10 and a mixture of LiOH/LiCl for pH(23 °C) 11 and 12. The SPFT experiments conducted under dilute conditions were also documented in a journal article (Pierce et al. 2008b).

Experiments with input solutions doped with Si (ranging from 15 to 140 ppm) were conducted as a function of temperature at pH(23 °C) = 9. The K_g for the disposal system temperature of 15 °C, which was determined in a similar fashion as LAWABP1, also is shown in Table 4.1. It should be noted that the K_g values for LAWA44, LAWB45, and LAWC22 listed in Table 4.1 are different from the values listed by Pierce et al. (2004), which are incorrect because of a calculation error. The calculation error was associated with the use of the molecular weight for H_4SiO_4 (96.11486 g/mol) instead of the molecular weight for Si (28.0855 g/mol) during the calculation of the Si activity. The difference between the reported K_g values in Pierce et al. (2004) and the values reported here is a factor of ~3.422. This error was identified first by

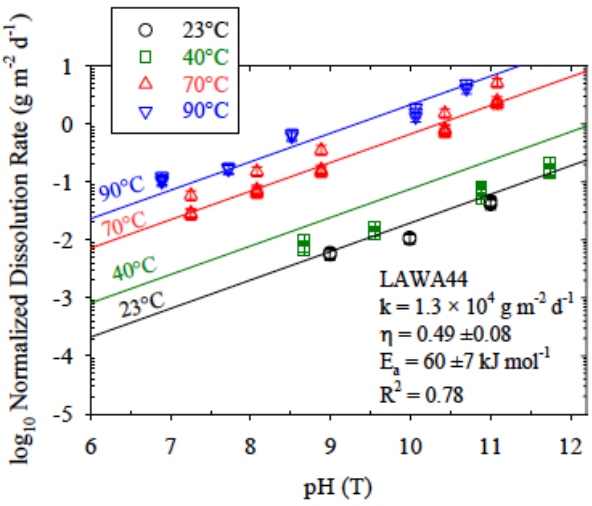

Figure 4.7. Normalized Glass Dissolution Rate, Based on Boron, as a Function of pH(T) for LAWA44 (from Pierce et al. 2004).

Papathanassiu et al. (2011). Therefore, the values listed in this report were adjusted by multiplying original values for LAWA44, LAWB45, and LAWC22 listed in Pierce et al. (2004) by ~3.422. The erroneous K_g values for LAWA44, LAWB45, and LAWC22 also were reported by Pierce et al. (2010a, 2011, 2013) and by Bacon and Pierce (2010).

The r_{IEX} typically decreases with an increase in the solution pH or temperature as matrix dissolution becomes the dominant mechanism of dissolution. Conversely, as the solution $SiO_2(aq)$ activity increases, the r_{IEX} mechanism becomes more influential because the ion activity product (Q) approaches saturation with respect to some secondary phase(s), and the rate of matrix dissolution slows, as shown for LAWABP1 in Figure 4.4. To estimate r_{IEX}, the steady-state Na release rate was subtracted from the steady-state matrix dissolution rate, indexed by boron, and the resulting value was converted to moles of Na per square meter per second. A linear regression of the data was used to compute the Na-r_{IEX} at 15 °C given in Table 4.1. LAWB45 exhibited little to no alkali hydrogen exchange, suggesting that matrix dissolution remained the dominant mechanism of release in the conditions tested. For this reason the value for r_{IEX} is given as "0" in Table 4.1. This is certainly due to the less than 6.5 wt% sodium loading for this glass formulation in comparison to the 20 wt% and 14 wt% for LAWA44 and LAWC22, respectively. In comparison to LAWA44 and LAWC22, LAWB45 not only has lower alkali content but also has higher Al and B content, resulting in a ratio of (Al+B)/(Na+Li+K) of 0.91 to 1. Hence, almost all of the alkali ions are used in charge compensating AlO_2^- and BO_2^- groups in the glass, reducing the concentration of non-bridging oxygen sites that are more susceptible to ion-exchange (McGrail et al. 2001a, b). As a result, a Na- r_{IEX} of zero is assigned to LAWB45 glass ($r_{IEX} = 0$).

Note that Table 4.1 collates data provided from several different reports. Hence, inconsistencies in significant digits and uncertainty reporting occur since data are reported as they were originally published. When ranges of values are reported (e.g., activation energy), the uncertainty represents a plus/minus standard deviation from the mean reported value.

Table 4.1. Summary of Rate Law Parameters for LD6-5412, LAWABP1, LAWA44, LAWB45, and LAWC22 at 15 °C

	Parameters							
	$\vec{k}_0$		K_g[(a)]	η	E_a	σ	r_{IEX}	
Glass	Reported Forward Rate Constant (g/[m^2 d])	Converted[(b)] Forward Rate Constant (mol/[m^2 s])	Glass Apparent Equilibrium Constant Based on Activity Product $a[SiO_2(aq)]$	pH Power Law Coefficient	Glass Dissolution Activation Energy (kJ/mol)	Temkin Coefficient	Na Ion-Exchange Rate (mol/[m^2 s])	Reference
LD6-5412	9.7×10^6	1.8×10^0	1.14×10^{-4}	0.40 ±0.03	74.8 ±1.0	1	1.74×10^{-11}[(c)]	McGrail et al. (1997)
LAWABP1	3.4×10^6	5.7×10^{-1}	4.90×10^{-4}	0.35 ±0.03	68 ±3.0	1	3.4×10^{-11}	McGrail et al. (2001a)
LAWA44	1.3×10^4 ($R^2 = 0.78$)	2.2×10^{-3}	1.87×10^{-3} ($R^2 = 0.95$)	0.49 ±0.08	60 ±7	1	5.3×10^{-11}	Pierce et al. (2004)
LAWB45	1.6×10^4 ($R^2 = 0.96$)	3.0×10^{-3}	1.79×10^{-3} ($R^2 = 0.78$)	0.34 ±0.03	53 ±3	1	0.0×10^0[(d)]	Pierce et al. (2004)
LAWC22	1.0×10^5 ($R^2 = 0.96$)	1.8×10^{-2}	1.80×10^{-3} ($R^2 = 0.94$)	0.42 ±0.02	64 ±2	1	1.2×10^{-10}	Pierce et al. (2004)

(a) The K_g value for LD6-5412 is from McGrail et al. (1997), which states that value for chalcedony should be used; value given is K_g at 15 °C for chalcedony from the Geochemist's Workbench database thermo.com.V8.R6+.dat (Aqueous Solutions LLC 2015). The K_g values for LAWA44, LAWB45, and LAWC22 listed in this report are different from the values listed in Pierce et al. 2004, which were subject to a calculation error as pointed out in Papathanassiu et al. (2011). The error was associated with the use of the molecular weight for H_4SiO_4 (96.11 g/mol) instead of the molecular weight for Si (28.09 g/mol) during the calculation of the Si activity, which resulted in a factor of ~3.422 miscalculation. The erroneous K_g values for LAWA44, LAWB45, and LAWC22 were also reported in Pierce et al. (2010a, 2011, 2013) and Bacon and Pierce (2010). The K_g values for LD6-5412 and LAWABP1 were reported accurately in their source documents.

(b) The converted forward rate constant (mol/[m^2 s]) is calculated from the reported forward rate constant (g/[m^2 d]) divided by molecular weight of the given glass from Table 2.1 and converting time from days to seconds.

(c) Ion exchange rate for LD6-5412 is reported in Mann et al. (2001).

(d) No detectable ion exchange rate for LAWB45.

5.0 Alteration Phases

IDF PA models should account for the formation of metastable, amorphous, and/or crystalline alteration phases during the glass-water reaction. This requires information on the glass transformation into a paragenetic assemblage of alteration products that make up the altered layers. Although the suite of products that will form because of the glass-water reactions cannot be determined *a priori* at this time, as discussed by McGrail et al. (1998a, 2000b, 2003) and Neeway et al. (2014a), a few methods are available to simulate the process. In this report, phases obtained using the product consistency test method B (PCT-B) (ASTM C1285-14) provides the alteration phase data relevant to the data package.

The PCT is a water-saturated static test that allows the reaction products to accumulate in the aqueous phase, thus altering the solution chemistry in contact with the glass. The PCT is an ASTM standard procedure (ASTM C1285-14) for testing nuclear, hazardous and mixed waste glass dissolution under static conditions. To obtain alteration phases that may form at longer times, PCT-B was performed at 90 °C and a variety of times, allowing the reaction products to accumulate in the aqueous phase and eventually form alteration products. The results have been documented in a series of reports (McGrail et al. 1997, 1998b, 2000a, 2001a; Pierce et al. 2004, 2010a, 2011, 2013, 2014; Pierce and Bacon 2011; Papathanassiu et al. 2011) and represent more than 260 different glass compositions that were tested for up to ~11 years. The vast majority of the glasses tested using PCT-B and the corresponding characterization were documented in Papathanassiu et al. (2011). Because this test is performed under near-static conditions[1], data obtained on the solution chemistry and alteration phases may differ from an open-system repository with flowing water at 15 °C.

An important outcome from experiments that represent glass corrosion in an open system (e.g., Pierce et al. 2006, 2007) is that ^{99}Tc is released from the glass matrix at the same rate as boron (e.g., Bibler and Jurgensen 1988) whereas uranium is retained in the alteration phases. Although alteration products formed from glass weathering can incorporate ^{99}Tc, its release can be represented conservatively in PA calculations by assuming that it is controlled by glass dissolution, and that secondary reactions do not influence the aqueous concentration of ^{99}Tc (Mattigod et al. 2002).

This section summarizes recent work on identifying potential alteration phases based on laboratory data and geochemical modeling. Additional data on potential alteration phases can be found in the ILAW 2005 data package (Pierce et al. 2004).

5.1 Geochemical Modeling Results

Geochemical modeling is needed to help identify potential alteration phases. Previous ILAW studies used the geochemical modeling program EQ3/6 (Wolery and Daveler 1992) to model experimental ILAW glass corrosion data for determining alteration phases that form during glass weathering. This section describes results of modeling performed on several glasses that are not specifically described in this document, but are provided as supplemental data to help identify alteration phases forming during the weathering of ILAW glasses.

[1] The PCT-B data reported in Papathanassiu et al. (2011) used a replacement technique where a small fraction of the leachate was replaced with deionized water at each sampling event.

To identify the correct mineral phases, it is necessary to eliminate many thermodynamically possible phases from consideration because 1) the formation of some phases is kinetically inhibited at the disposal system temperature of 15 °C, 2) the selection of some phases will violate the Gibbs phase rule, 3) simulations will be compared with experiments, and phases will be eliminated that generated solution compositions that were inconsistent with the experiments, or 4) there is phase instability over the range of chemical conditions expected for the ILAW disposal system. The bulk of the final set of phases appropriate for each glass type will be determined by simulating the solution chemistry observed in PCT experiments. For additional details on the modeling approach, see Pierce et al. (2010a, 2011, and 2013).

Classical geochemical reaction path modeling codes, such as Geochemist's Workbench and EQ3/6, integrate macroscopic reaction kinetics with equilibrium thermodynamics and are based on the principles of mass balance, equilibrium thermodynamics between species, and kinetic rate laws for mass transfer. The equilibrium thermodynamics provide the system limits required to describe the evolution of the bulk solution chemistry by capturing the thermodynamic constraints associated with secondary phase formation. In the case of the glass-water reaction, the following assumptions were made: 1) dissolution of the glass is a rate-limiting, irreversible reaction and the driver for the geochemistry of the system, 2) precipitation of alteration phases is instantaneous, 3) the aqueous solution is at equilibrium with or undersaturated with respect to all secondary minerals at all times, 4) fluid chemistry obeys the Gibbs phase rule, and 5) alteration phases dissolve and precipitate in a paragenetic sequence as the aqueous chemistry evolves. Although these simulations for the glass water reaction are largely successful, there are limitations to these simulations.

The limitations associated with this modeling approach center on the need to combine data from bulk solution chemistry and *ex situ* solid-phase characterization techniques to understand the time-dependent changes that occur between the reacting glass and the developing alteration layer. As a result, several intermediate steps, which represent the steady-state element concentrations measured in experiments, are not explicitly represented. For example, the formation of intermediate phases, whether amorphous or crystalline, can significantly affect the evolution of the aqueous chemistry. Additionally, equations that accurately describe the complex processes that govern nucleation and growth kinetics, which will influence the solution chemistry and alteration phase formation, are also needed and must be coupled to intermediate phase formation. Amorphous intermediate phases are the rule rather than the exception for glass systems, and a few of the assigned crystalline phases simply represent close proxies of observed mineral phases that typically deviate from the idealized stoichiometries contained in the thermodynamic database.

In addition to the computer simulations, alteration products are characterized to identify key secondary phases that are required to constrain the computer simulations. Alteration products formed at the surfaces of the glass in the PCT experiments are characterized by x-ray diffraction (XRD), scanning electron microscopy/energy dispersive spectroscopy (SEM/EDS), and transmission electron microscopy; however, only the results of XRD and SEM/EDS are presented here. For more detail on the uncertainty associated with this approach, see Pierce et al. (2014).

Modeling of 128 different glass compositions was conducted in fiscal year (FY) 2011 (Pierce et al. 2011) and an additional 10 glass compositions were modeled in FY 2012 (Pierce et al. 2013). Initial modeling of the PCT results for the 138 glass samples was conducted using the secondary phases listed in Table 5.1. These alteration phases are the same as those identified for LAWA44 by Pierce et al. (2004). In a number of cases, the log K values from the original EQ 3/6 database were adjusted to get the values

shown in Table 5.1 to adequately reproduce the PCT solution concentration data. This involved a shift in the log K value to account for the formation of amorphous solids, as well as an adjustment for the temperature dependence of the equilibrium constant. For the former, upward adjustments of the log K values were used because amorphous phases rather than their crystalline analogs often form in laboratory experiments with waste glasses. Amorphous solids are typically much more soluble than their crystalline analogs. For example according to the Geochemist's Workbench database thermo.com.V8.R6+.dat[1] (Aqueous Solutions LLC 2015), amorphous silica (log K @ 25 °C = $10^{-2.7136}$) is more soluble than quartz (log K @ 25 °C = $10^{-3.993}$). For the latter, the log K can be adjusted based on the following equation:

$$\log K_{eq} = a_{eq} \ln T + b_{eq} + c_{eq}T + \frac{d_{eq}}{T} + \frac{e_{eq}}{T^2} \quad (5.1)$$

where T is the temperature in degrees kelvin, and a_{eq}, b_{eq}, c_{eq}, d_{eq}, and e_{eq} are fitting coefficients that can be obtained from geochemical databases (e.g., EQ3/6, Geochemist's Workbench). Once the log K is interpolated to 90 °C, a shift factor (S_f) is applied to account for the formation of amorphous solids that form in laboratory experiments, as precursors to crystalline equivalents. Eq. (5.1) is further modified to account for the shift factor as shown in Eq. (5.2).

$$\log K_{eq} = a_{eq} \ln T + b_{eq} + c_{eq}T + \frac{d_{eq}}{T} + \frac{e_{eq}}{T^2} + S_f \quad (5.2)$$

Table 5.1 shows the log K values for the alteration phases at 90 °C. Data used to obtain these log K values were obtained from the Geochemist's Workbench database thermo.com.V8.R6+.dat (Aqueous Solutions LLC 2015) and are shown in Table 5.2. Since PA calculations will be performed at 15 °C, log K values are provided in Table 5.3 using Eq. 5.2 and assuming the same shift values. Data in Table 5.2 were also used to obtain the equilibrium coefficients (log values) at 15 °C.

The usefulness of this approach can be visually appreciated in the co-plotted experimental solution concentrations and model results found in Pierce et al. (2011) and Pierce et al. (2013), although the errors were not calculated. Some key discrepancies include intermittent Ca disagreement and predicted concentrations for K and Li generally higher than measured concentrations. This suggests that this work is as yet incomplete and that more attention is warranted, but that the general approach is effective at modeling the incongruent solution concentration changes observed in the data for a large number of glass compositions.

[1] A specific version (8.0.12) of Geochemist's Workbench has been approved at PNNL under the WWFTP QA program (which implements NQA-1-2008/NQA-1a-2009 QA requirements). The scope of approved use of Geochemist's Workbench 8.0.12 is limited to geochemical equilibrium modeling for conditions consistent with the thermodynamic database that was used to test and qualify the software, as documented on in PNNL's Software Control Package (SCP), SCP-62815-001, Rev. 0.

Table 5.1. Alteration Phases Used for Initial Modeling of PCT Results at 90 °C (Pierce et al. 2011)

Phase	Reaction	Log K (90°C)
Analcime ($Na_{0.96}Al_{0.96}Si_{2.04}O_6•H_2O$)	Analcime + $3.84H^+ \leftrightarrow 0.96Al^{3+} + 0.96Na^+ + 2.04SiO_2(aq) + 2.92H_2O$	3.40
Anatase (TiO_2)	$TiO_2 + 2H_2O \leftrightarrow Ti(OH)_4(aq)$	-6.56
Baddeleyite (ZrO_2)	$ZrO_2 + 2H^+ \leftrightarrow Zr(OH)_2^{2+}$	-5.20
Calcite ($CaCO_3$)	$CaCO_3 + H^+ \leftrightarrow Ca^{2+} + HCO_3^-$	0.91
Chalcedony (SiO_2)	$SiO_2 \leftrightarrow SiO_2(aq)$	-2.65
$Fe(OH)_3(s)$	$Fe(OH)_3(am) + 3H^+ \leftrightarrow Fe^{3+} + 3H_2O$	3.04
Gibbsite [$Al(OH)_3$]	$Al(OH)_3 + 3H^+ \leftrightarrow Al^{3+} + 3H_2O$	4.46
Sepiolite [$Mg_4Si_6O_{15}(OH)_2•6H_2O$]	Sepiolite + $8H^+ \leftrightarrow 4Mg^{2+} + 6SiO_2(aq) + 11H_2O$	39.72
$Zn(OH)_2$-γ	$Zn(OH)_2$-γ + $2H^+ \leftrightarrow Zn^{2+} + 2H_2O$	11.88

Table 5.2. Fitting Coefficients and Shift Values Used to Obtain Log K Values at Different Temperatures

Phase	*a*	*b*	*c*	*d*	*e*	Shift
Analcime ($Na_{0.96}Al_{0.96}Si_{2.04}O_6•H_2O$)	3.07E+02	-2.01E+03	-2.50E-01	1.31E+05	-8.60E+06	0.00E+00
Anatase (TiO_2)	0.00	-8.56E+00	0.00	0.00	0.00	2.00E+00
Baddeleyite (ZrO_2)	-8.84E+00	5.40E+01	2.28E-03	-4.36E+03	2.11E+05	2.50E+00
Calcite ($CaCO_3$)	1.42E+02	-9.04E+02	-1.44E-01	5.07E+04	-2.93E+06	0.00E+00
Chalcedony (SiO_2)	1.01E+02	-6.66E+02	-7.48E-02	4.38E+04	-3.28E+06	3.00E-01
$Fe(OH)_3(s)$	8.33E+01	-5.35E+02	-8.25E-02	3.24E+04	-1.56E+06	0.00E+00
Gibbsite [$Al(OH)_3$]	6.95E+01	-4.44E+02	-7.84E-02	2.77E+04	-1.28E+06	0.00E+00
Sepiolite [$Mg_4Si_6O_{15}(OH)_2•6H_2O$]	8.42E+02	-5.51E+03	-6.61E-01	3.61E+05	-2.39E+07	1.50E+01
$Zn(OH)_2$-γ	0.00	1.19E+01	0.00	0.00	0.00	0.00E+00

Table 5.3. Principal Alteration Phase Log K Values at 15 °C

Phase	Reaction	Log K (15 °C)
Analcime ($Na_{0.96}Al_{0.96}Si_{2.04}O_6•H_2O$)	Analcime + $3.84H^+ \leftrightarrow 0.96Al^{3+} + 0.96Na^+ + 2.04SiO_2(aq) + 2.92H_2O$	6.55
Anatase (TiO_2)	$TiO_2 + 2H_2O \leftrightarrow Ti(OH)_4(aq)$	-6.56
Baddeleyite (ZrO_2)	$ZrO_2 + 2H^+ \leftrightarrow Zr(OH)_2^{2+}$	-5.50
Calcite ($CaCO_3$)	$CaCO_3 + H^+ \leftrightarrow Ca^{2+} + HCO_3^-$	2.00
Chalcedony (SiO_2)	$SiO_2 \leftrightarrow SiO_2(aq)$	-3.64
$Fe(OH)_3(s)$	$Fe(OH)_3(am) + 3H^+ \leftrightarrow Fe^{3+} + 3H_2O$	6.16
Gibbsite [$Al(OH)_3$]	$Al(OH)_3 + 3H^+ \leftrightarrow Al^{3+} + 3H_2O$	8.37
Sepiolite [$Mg_4Si_6O_{15}(OH)_2•6H_2O$]	Sepiolite + $8H^+ \leftrightarrow 4Mg^{2+} + 6SiO_2(aq) + 11H_2O$	46.27
$Zn(OH)_2$-γ	$Zn(OH)_2$-γ + $2H^+ \leftrightarrow Zn^{2+} + 2H_2O$	11.88

5.2 Solid-Phase Characterization Results

Selected glass samples from the PCT tests were also characterized with XRD and SEM/EDS. Of the phases identified by XRD, thermodynamic data are available only for analcime, saponite, and foshagite. Other methods (e.g., using standard Gibbs free energy of reaction and temperature) can be used to estimate equilibrium constants. For additional details on the XRD and SEM/EDS results, see Papathanassiu et al. (2011).

The most common phase identified in the samples was analcime [$Na(AlSi_2O_6)(H_2O)$]. This phase was frequently the second most abundant phase predicted to occur in the reaction progress modeling (after chalcedony). Using the initial alteration phases, analcime was predicted to occur in the PCTs for all samples.

Table 5.4 summarizes the minerals identified in both SEM/EDS and XRD analyses on a wide variety of glasses, as well as the number of occurrences in the analyzed samples (details on the mineral identification correspondence to each glass sample can be found in Appendix A).

For the SEM/EDS analyses, evidence supporting the possible presence of a number of phases (saponite, $Fe(OH)_3$, $Zn(OH)_2$, $Zr(OH)_4$, phillipsite, and stevensite and a calcium silicate phase) is less certain because the method does not provide information on crystalline structure. It is highly likely that these minerals are amorphous and/or crystallographically different for the listed phase, and thus they are listed with a "possible" identifier in Table 5.4.

Table 5.4. Additional Alteration Phases

Phase	XRDSamples	SEM/EDS Samples
Gobbinsite [$Na_5(Si_{11}Al_5)O_{32}$•$11H_2O$]	2	---
Stevensite [$(Ca,Na)_xMg_{3-x}Si_4O_{10}(OH)_2$]	7	Possible
Hectorite-15a [$Na_{0.2}(Mg,Li)_3Si_4O_{10}(OH)_2$•$4H_2O$]	1	---
Phillipsite-Na [$Na_4KAl_5Si_{11}O_{32}(H_2O)_{10}$]	1	Possible
Chabazite [$Ca_2Al_4Si_8O_{24}$•$12H_2O$]	3	10
Herschelite [$NaAlSi_2O_6$•$3H_2O$]	2	---
Saponite-15Å [$Ca_{0.2}Mg_3(SiAl)_4O_{10}(OH)_2$•$4H_2O$]	1	Possible
Swinfordite-13Å [$Ca_{0.1}(Li,Al)_3Si_4O_{10}(OH)_2$•$2H_2O$]	3	---
Foshagite [$Ca_4(SiO_3)_3(OH)_2$]	1	Possible
Iron Hydroxide [$Fe(OH)_3$]	---	Possible
Zinc Hydroxide [$Zn(OH)_2$]	---	Possible
Zirconium Hydroxide [$Zr(OH)_4$]	---	Possible

6.0 Summary

Currently, DOE plans to dispose of the glasses made from nuclear waste stored in underground tanks at Hanford at two U.S. locations: 1) the ILAW glass will be stored on site at the IDF and 2) the immobilized HLW glass will be placed into a federal geologic repository. The solid and liquid waste recovered from the tanks will be pretreated to separate the low-activity fraction from the high-level and transuranic waste fractions. The LAW and HLW fractions will be separately immobilized into vitrified matrices (i.e., borosilicate glasses).

Before the immobilized low-activity waste can be placed into the disposal system, DOE must approve a performance assessment (PA), which documents the assumptions and provides the quantitative demonstration of compliance with the performance objectives for the long-term protection of the public and the environment. A critical component of the 2017 PA will be to demonstrate that releases from the selected glass waste form do not result in the performance objectives being exceeded. The PA provides reasonable assurance that the facility design and method of disposal will comply with the performance objectives of DOE order 435.1, which ensure protection of public health and safety in limiting doses to members of the public and limiting releases of radon. The PA must also, for purposes of establishing limits on radionuclides that may be buried near-surface, assess impacts to a hypothetical intruder and impacts to water resources.

This data package provides a general discussion on nuclear waste glass corrosion and a brief overview of a reactive transport modeling approach. However, the key information presented in this data package consists of the specific glass compositions and rate law parameters for five ILAW glasses to be used to support the 2017 PA. In addition, end-point alteration phases are provided for several glasses to help identify potential alteration phases. Tables presented in this data package provide the specific data (glass compositions, rate law parameters, and alteration phases) to be used to support the 2017 PA.

Future iterations of the IDF PA data package are expected to include additional performance data from tests on enhanced or advanced glasses (e.g., Muller et al. 2010; Muller et al. 2014; Vienna et al. 2013b). The enhanced or advanced LAW glass compositions seek to optimize waste loading (e.g., increasing Na_2O concentration in glass to reduce the total volume of glass for disposal). Although there has been a significant amount of testing performed on these higher waste loading glasses, there is limited data available to support the FY17 PA (e.g., limited SPFT have been performed from which rate law parameters can be attained). Therefore, data for these glasses are not presented in this report.

7.0 References

ASTM C1663-09, *Standard Test Method for Measuring Waste Glass or Glass Ceramic Durability by Vapor Hydration Test*. ASTM International, West Conshohocken, Pennsylvania.

ASTM C1662-10, *Standard Practice for Measurement of the Glass Dissolution Rate Using the Single-Pass Flow-Through Test Method*. ASTM International, West Conshohocken, Pennsylvania.

ASTM C1285-14, *Standard Test Methods for Determining Chemical Durability of Nuclear, Hazardous, and Mixed Waste Glasses and Multiphase Glass Ceramics: The Product Consistency Test (PCT)*. ASTM International, West Conshohocken, Pennsylvania.

Abraitis PK, FR Livens, JE Monteith, JS Small, DP Trivedi, DJ Vaughan, and RA Wogelius. 2000. "The Kinetics and Mechanisms of Simulated British Magnox Waste Glass Dissolution as a Function of pH, Silicic Acid Activity, and Time in Low-Temperature Aqueous Systems." *Applied Geochemistry* **15**:1399−1416.

Aqueous Solutions LLC. 2015. thermo.com.V8.R6+.dat database (older format), *July 24, 2015*. http://www.gwb.com/data/Old_format/thermo.com.V8.R6+.dat

Bacon DH, and EM Pierce. 2010. *Sensitivity Analysis of Kinetic Rate-Law Parameters Used to Simulate Long-Term Weathering of ILAW Glass*. PNNL-19472, Pacific Northwest National Laboratory, Richland, Washington.

Bibler NE and AR Jurgensen. 1988. "Leaching Tc-99 from SRP Glass in Simulated Tuff and Salt Groundwaters," Scientific Basis for Nuclear Waste Management, XI, M.J. Apted and R.E. Westerman (eds.), Materials Research Society, Pittsburgh, PA, 1988, pp. 585–593.

Boksay Z, G Bouquet, and S Dobos. 1968. "Kinetics of Formation of Leached Layers on Glass Surfaces." *Physics and Chemistry of Glasses* **9** (2):69-71.

Bunker BC, GW Arnold, and EK Beauchamp. 1983. "Mechanisms for Alkali Leaching in Mixed-Na-K-Silicate Glasses." *Journal of Non-Crystalline Solids* **58**:295−322.

Bunker BC, GW Arnold, DE Day, and PJ Bray. 1986. "The Effect of Molecular Structure on Borosilicate Glass Leaching." *Journal of Non-Crystalline Solids* **87**:226−253.

Bunker BC, DR Tallant, TJ Headley, GL Turner, and RJ Kirkpatrick. 1988. "The Structure of Leached Sodium Borosilicate Glass." *Physics and Chemistry of Glasses* **29** (3):106−120.

Bunker BC. 1994. "Molecular Mechanisms for Corrosion of Silica and Silicate Glasses." *Journal of Non-Crystalline Solids* **179**:300−308.

Casey WH, and BC Bunker. 1990. "Leaching of Mineral and Glass Surfaces During Dissolution." In *Reviews in Mineralogy, vol. 23*, edited by MF Hochella Jr. and AF White, 397−426. Mineralogical Society of America.

Certa PJ and MN Wells. 2010. *River Protection Project System Plan*. ORP-11242, Rev. 5, U.S. Department of Energy, Office of River Protection, Richland, Washington.

Chen Y, DW Engel, BP McGrail, and KS Lessor. 1995. *AREST-CT V1.0 Software Verification*. PNL-10692, Pacific Northwest Laboratory, Richland, Washington.

Chen Y, BP McGrail, and DW Engel. 1997. "Source-Term Analysis for Hanford Low-Activity Tank Waste using the Reaction-Transport Code AREST-CT." In *Scientific Basis for Nuclear Waste Management XX*. Pittsburgh, Pennsylvania.

Cunnane JC, JK Bates, and CR Bradley. 1994a. *High-Level Waste Borosilicate Glass: A Compendium of Corrosion Characteristics, Vol. 1*. DOE-EM-0177, U.S. Department of Energy, Office of Waste Management, Springfield, Virginia.

Cunnane JC, JK Bates, and CR Bradley. 1994b. *High-Level Waste Borosilicate Glass: A Compendium of Corrosion Characteristics, Vol. 2*. DOE-EM-0177, U.S. Department of Energy, Office of Waste Management, Springfield, Virginia.

DOE. 1988. *Radioactive Waste Management*. DOE Order 5820.2A, U.S. Department of Energy, Washington, D.C.

DOE. 1998. *Radioactive Waste Management*. DOE Order 435.1-1, U.S. Department of Energy, Washington, D.C.

DOE. 1999. *Final Report for the Hanford Site 200 Area Plateau Composite Analysis and the Immobilized Low-Activity Tank Waste*. U.S. Department of Energy, Richland, Washington.

DOE. 2000. *Design, Construction, and Commissioning of the Hanford Tank Waste Treatment and Immobilization Plant*. Contract DE-AC27-01RV14136, as amended, U.S. Department of Energy, Office of River Protection, Richland, Washington.

DOE. 2001. *Final Review Team Report for the March 2001 Revision of the Hanford Immobilized Low-Activity Waste Performance Assessment*. U.S. Department of Energy, Richland, Washington.

Doremus RH. 1975. "Interdiffusion of Hydrogen and Alkali Ions in a Glass Surface." *Journal of Non-Crystalline Solids* **19**:137−144.

Ebert WL. 2014. An Evaluation of the ALTGLASS Database for Insights into Modeling Stage 3 Behavior. Technical Rpt. FCRD-SWF-2014-000616, U.S. Department of Energy, Washington, D.C.

Feng X and IL Pegg. 1994a. "A Glass Dissolution Model for the Effects of S/V on Leachate pH." *Journal of Non-Crystalline Solids* **175**(2−3):281−293.

Feng X and IL Pegg. 1994b. "Effects of Salt Solutions on Glass Dissolution." Physics and Chemistry of Glasses **35**:98–103.

Frugier P, T Chave, S Gin, and JE Lartigue. 2009. "Application of GRAAL Model to Leaching Experiments with SON68 Nuclear Glass in Initially Pure Water." *Journal of Nuclear Materials* **392**(3):552-567.

Geisler T, A Janssen, D Scheiter, T Stephan, J Berndt, and A Putnis. 2010. "Aqueous Corrosion of Borosilicate Glass under Acidic Conditions: A new corrosion mechanism." *Journal of Non-Crystalline Solids* **356** (28–30):1458−1465. doi: http://dx.doi.org/10.1016/j.jnoncrysol.2010.04.033.

Gin S and JP Mestre. 2001. "SON 68 Nuclear Glass Alteration Kinetics between pH 7 and pH 11.5." *Journal of Nuclear Materials* **295**:83−96.

Gin S, A Abdelouas, LJ Criscenti, WL Ebert, K Ferrand, T Geisler, MT Harrison, Y Inagaki, S Mitsui, KT Mueller, JC Marra, CG Pantano, EM Pierce, JV Ryan, JM Schofield, CI Steefel, and JD Vienna. 2013. "An International Initiative on Long-term Behavior of High-Level Nuclear Waste Glass." *Materials Today* **16**(6):243−248.

Grambow B. 1985. "A General Rate Equation for Nuclear Waste Glass Corrosion." *Materials Research Society Symposium Proceedings* **44**:15−27.

Grambow B, W Lutze, E Vernaz, and GG Wicks. 2000. *Final Report - Peer Review Committee (PRC) Assessment of the Proposed Long-Term Performance Strategy for Hanford Immobilized Low Activity Waste (ILAW) (U)*. WSRC-RP-2000-00876, Westinghouse Savannah River Company, Aiken, South Carolina.

Hamilton JP, SL Brantley, CG Pantano, LJ Criscenti, and JD Kubicki. 2001. "Dissolution of Nepheline, Jadeite and Albite Glasses: Toward Better Models for Aluminosilicate Dissolution." *Geochimica Et Cosmochimica Acta* **65**(21):3683−3702.

Hellman R, S Cotte, E Cadel, S Malladi, LS Karlsson, S Lozano-Perez, M Cabie, and A Seyeux. 2015. "Nanometre-Scale Evidence for Interfacial Dissolution-Reprecipitation Control of Silicate Glass Corrosion." *Nature Materials* **14**:307−311. doi:10.1038/NMAT4172.

Icenhower JP, BP McGrail, WJ Shaw, EM Pierce, P Nachimuthu, DK Shuh, EA Rodriguez, and JL Steele. 2008. "Experimentally Determined Dissolution Kinetics of Na-rich Borosilicate Glass at far from Equilibrium Conditions: Implications for Transition State Theory." *Geochimica Et Cosmochimica Acta* **72**(12):2767−2788.

Icenhower JP, BP McGrail, and A Luttge. 2002. "Origins of Deviations from Transition-State Theory: Effects of Ion-Exchange Kinetics in Glass." *Geochimica Et Cosmochimica Acta* **66** (15A):A351−A351.

Icenhower JP, S Samson, A Luttge, and BP McGrail. 2004. "Towards a Consistent Rate Law: Glass Corrosion Kinetics Near Saturation." In *Energy, Waste, and the Environment: A Geochemical Perspective*, edited by R Giere and P Stille, 579−594. Geological Society of London.

Jantzen CM, DI Kaplan, NE Bibler, DK Peeler, and MJ Plodinec. 2008. "Performance of a Buried Radioactive High-Level Waste (HLW) Glass after 24 Years." *Journal of Nuclear Materials* **378**:244−256.

Mann FM. 1995a. *Computer Code Selection Criteria and Considerations for the Hanford Low-Level Waste Interim Performance Assessment*. WHC-SD-WM-CSWD-073, Westinghouse Hanford Company, Richland, Washington.

Mann FM. 1995b. *Data Packages for the Hanford Low-Level Tank Waste Interim Performance Assessment*. WHC-SD-WM-RPT-166, Rev. 0, Westinghouse Hanford Company, Richland, Washington.

Mann FM. 1995c. *Scenarios of the TWRS Low-Level Waste Disposal Program*. WHC-EP-0828, Rev. 1, Westhinghouse Hanford Company, Richland, Washington.

Mann FM. 1995d. *Performance Objectives of the Tank Waste Remediation System Low-Level Waste Disposal Program*. WHC-EP-0826, Rev. 1, Westinghouse Hanford Company, Richland, Washington.

Mann FM, CR Eiholzer, R Khaleel, NW Kline, AH Lu, BP McGrail, PD Rittmann, and F Schmittroth. 1995. *Definition of the Base Analysis Case of the Interim Performance Assessment*. WHC-SD-WM-RPT-200, Rev. 0, Westinghouse Hanford Company, Richland, Washington.

Mann FM, CR Eiholzer, AH Lu, PD Rittmann, NW Kline, Y Chen, and BP McGrail. 1996. *Hanford Low-Level Tank Waste Interim Performance Assessment*. WHC-EP-0884, Rev. 0, Westinghouse Hanford Company, Richland, Washington.

Mann FM. 1997. *Statements of Work for FY 1998 to 2003 for the Hanford Low-Level Tank Waste Performance Assessment Project*. Richland, Washington.

Mann FM, RJ Puigh II, CR Eiholzer, Y Chen, NW Kline, AH Lu, BP McGrail, PD Rittmann, GF Williamson, NR Brown, and PE LaMont. 1998. *Hanford Immobilized Low Activity Tank Waste Performance Assessment*. DOE/RL-97-69 Rev. B, Project Hanford Management Contractor, Richland, Washington.

Mann FM and DA Myers. 1998. *Computer Code Selection Criteria for Flow and Transport Code(s) to Be Used in Undisturbed Vadose Zone Calculations for TWRS Environmental Analyses*. HNF-1839, Rev. 0, Richland, Washington.

Mann FM, KC Burgard, WR Root, RJ Puigh, SH Finfrock, R Khaleel, DH Bacon, EJ Freeman, BP McGrail, SK Wurstner, and PE LaMont. 2001. *Hanford Immobilized Low-Activity Waste Performance Assessment: 2001 Version*. DOE/ORP-2000-24 Rev. 0, U.S. Department of Energy, Office of River Protection, Richland, Washington.

Mattigod SV, RJ Serne, BP McGrail, and VL Legore. 2002. "Radionuclide Incorporation in Secondary Crystalline Minerals From Chemical Weathering of Waste Glasses." Paper read at Scientific Basis for Nuclear Waste Management, Boston, Massachusetts.

Meyer PD and RJ Serne. 1999. *Near-Field Hydrology Data Package for the Immobilized Low-Activity Waste 2001 Performance Assessment*. PNNL-13035, Pacific Northwest National Laboratory, Richland, Washington.

Meyer PD, P Saripalli and VL Freedman. 2004. *Near-Field Hydrology Data Package for the Integrated Disposal Facility 2005 Performance Assessment*. PNNL-14700, Pacific Northwest National Laboratory, Richland, Washington.

McGrail BP, WL Ebert, AJ Bakel, and DK Peeler. 1997. "Measurement of Kinetic Rate Law Parameters on a Na-Ca-Al Borosilicate Glass for Low-Activity Waste." *Journal of Nuclear Materials* **249**(2–3):175–189.

McGrail BP, DH Bacon, WL Ebert, and KP Saripalli. 1998a. *A Strategy to Conduct an Analysis of the Long-Term Performance of Low-Activity Waste Glass in a Shallow Subsurface Disposal System at Hanford*. PNNL-11834, Pacific Northwest National Laboratory, Richland, Washington.

McGrail BP, PF Martin, CW Lindenmeier, and HT Schaef. 1998b. *Corrosion Testing of Low-Activity Waste Glasses: Fiscal Year 1998 Summary Report*. PNNL-12014, Pacific Northwest National Laboratory, Richland, Washington.

McGrail BP and DH Bacon. 1998. *Selection of a Computer Code for Hanford Low-Level Waste Engineered Performance Assessment*. PNNL-10830 Rev 1, Pacific Northwest National Laboratory, Richland, Washington.

McGrail BP, JP Icenhower, DH Bacon, JD Vienna, A Jiricka, WL Ebert, PF Martin, HT Schaef, MJ O'Hara, and EA Rodriguez. 1999. *Waste Form Release Data Package for the 2001 Immobilized Low-Activity Waste Performance Assessment*. PNNL-13043, Rev. 1, Pacific Northwest National Laboratory, Richland, Washington.

McGrail BP, JP Icenhower, PF Martin, DR Rector, HT Schaef, EA Rodriguez, and JL Steele. 2000a. *Low-Activity Waste Glass Studies: FY2000 Summary Report*. PNNL-13381, Pacific Northwest National Laboratory, Richland, Washington.

McGrail BP, DH Bacon, WL Ebert, and KP Saripalli. 2000b. *A Strategy to Conduct an Analysis of the Long-Term Performance of Low-Activity Waste Glass in a Shallow Subsurface Disposal System at Hanford*. PNNL-11834 Rev. 1, Pacific Northwest National Laboratory, Richland, Washington.

McGrail BP, DH Bacon, JP Icenhower, WL Ebert, PF Martin, HT Schaef, and EA Rodriguez. 2001a. *Waste Form Release Data Package for the 2001 Immobilized Low-Activity Waste Performance Assessment*. PNNL-13043, Rev. 2, Pacific Northwest National Laboratory, Richland, Washington.

McGrail BP, DH Bacon, JP Icenhower, FM Mann, RJ Puigh, HT Schaef, and SV Mattigod. 2001b. "Near-Field Performance Assessment for a Low-Activity Waste Glass Disposal System: Laboratory Testing to Modeling Results." *Journal of Nuclear Materials* **298**:95−111.

McGrail BP, JP Icenhower, DK Shuh, P Liu, JG Darab, DR Baer, S Thevuthasen, V Shutthanandan, MH Engelhard, CH Booth, and P Nachimuthu. 2001c. "The Structure of Na_2O-Al_2O_3-SiO_2 Glass: Impact on Sodium Ion Exchange in H_2O and D_2O." *Journal of Non-Crystalline Solids* **296**:10−26.

McGrail BP, DH Bacon, RJ Serne, and EM Pierce. 2003. *A Strategy to Assess Performance of Selected Low-Activity Waste Forms in an Integrated Disposal Facility*. PNNL-14362, Pacific Northwest National Laboratory, Richland, Washington.

Mišíková L, M Liška, D Galusková. 2007. "Corrosion of e-glass fibers in distilled water", *Ceramics − Silikáty* **51** (3), 131-135.

Muller IS, AC Buechele, and IL Pegg. 2001. *Glass Formulation and Testing with RPP-WTP-LAW Simulants.* VSL-01R3560-2, Vitreous State Laboratory, The Catholic University of America, Washington, D.C.

Muller IS, KS Matlack, H Gan, I Joseph, and IL Pegg. 2010. *Waste Loading Enhancements for Hanford LAW Glasses, Final Report*. VSL-10R1790-1, Rev. 0, Vitreous State Laboratory, The Catholic University of America, Washington, D.C.

Muller IS, K Gilbo, I Joseph, and IL Pegg. 2014. *Enhanced LAW Glass Property-Composition Models, Phase 2, Final Report*. VSL-14R3050-1. Vitreous State Laboratory, The Catholic University of America, Washington, D.C.

Nagy KL and AC Lasaga. 1993. "Letter: Simultaneous Precipitation Kinetics of Kaolinite and Gibbsite at 80°C and pH 3." *Geochimica et Cosmochimica Acta* **57**:4329−4335.

Nagy KL. 1995. "Dissolution and Precipitation Kinetics of Sheet Silicates." In *Chemical Weathering Rates of Silicate Minerals. Reviews in Mineralogy*, edited by AF White and SL Brantley, 173−233. Washington, D.C.: Mineralogical Society of America.

Neeway JJ, EM Pierce, VL Freedman, JV Ryan, and NP Qafoku. 2014a. *A Strategy to Conduct an Analysis of the Long-Term Performance of Low-Activity Waste Glass in a Shallow Subsurface Disposal System at Hanford*. PNNL-23503, Pacific Northwest National Laboratory, Richland, Washington.

Neeway JJ, S Kerisit, SP Gin, Z Wang, Z Zhu, and JV Ryan. 2014b. "Low-Temperature Lithium Diffusion in Simulated High-Level Boroaluminosilicate Nuclear Waste Glasses." *Journal of Non-Crystalline Solids* **405**:83−90.

Papathanassiu A, IS Muller, M Brandys, K Gilbo, A Barkatt, I Joseph, and IL Pegg. 2011. *ILAW Glass Testing for Disposal at IDF: Phase 1 Testing*. VSL-11R2270-1, Vitreous State Laboratory, The Catholic University of America Washington, D.C.

Pederson LR, DR Baer, GL McVay, and MH Engelhard. 1986. "Reaction of soda lime silicate glass in isotopically labelled water." *Journal of Non-Crystalline Solids* **86**:369−380.

Pierce EM, BP McGrail, EA Rodriguez, HT Schaef, KP Saripalli, RJ Serne, KM Krupka, PF Martin, SR Baum, KN Geiszler, LR Reed, and WJ Shaw. 2004. *Waste Form Release Data Package for the 2005 Integrated Disposal Facility Performance Assessment*. PNNL-14805, Pacific Northwest National Laboratory, Richland, Washington.

Pierce EM, BP McGrail, MM Valenta, and DM Strachan. 2006. "The accelerated weathering of a radioactive low-activity waste glass under hydraulically unsaturated conditions: Experimental results from a pressurized unsaturated flow test." *Nuclear Technology* **155**:149−165.

Pierce EM, BP McGrail, J Marra, PF Martin, BW Arey, and KN Geiszler. 2007. "Accelerated Weathering of a High-Level and Pu-bearing Lanthanide Borosilicate Waste Glass in a Can-in-Canister Configuration." *Applied Geochemistry* **22**:1841−1859.

Pierce EM, EL Richards, AM Davis, LR Reed, and EA Rodrigueza. 2008a. "Aluminoborosilicate Waste Glass Dissolution under Alkaline Conditions at 40°C: Implications for a Chemical Affinity-based Rate Equation." *Environmental Chemistry* **5**:1–13.

Pierce EM, EA Rodriguez, LJ Calligan, WJ Shaw, and BP McGrail. 2008b. "An Experimental Study of the Dissolution Rates of Simulated Aluminoborosilicate Waste Glasses as a Function of pH and Temperature under Dilute Conditions." *Applied Geochemistry* **23**:2559−2573.

Pierce EM, DH Bacon, SN Kerisit, CF Windisch, KJ Cantrell, MM Valenta, SD Burton, RJ Serne, and SV Mattigod. 2010a. *Integrated Disposal Facility Glass Testing FY2010 Summary Report*. PNNL-19736, Pacific Northwest National Laboratory, Richland, Washington.

Pierce EM, LR Reed, WJ Shaw, BP McGrail, JP Icenhower, CF Windisch, EA Cordova, and J Broady. 2010b. "Experimental Determination of the Effect of the Ratio of B/Al on Glass Dissolution Along the Nepheline ($NaAlSiO_4$)–Malinkoite ($NaBSiO_4$) Join." *Geochimica et Cosmochimica Acta* **74**:2634−2654.

Pierce EM, DH Bacon, SN Kerisit, CF Windisch, KJ Cantrell, MM Valenta, and SD Burton. 2011. *Integrated Disposal Facility Glass Testing FY2011 Summary Report*. PNNL-20781, Pacific Northwest National Laboratory, Richland, Washington.

Pierce EM and DH Bacon. 2011. "Combined Experimental and Computational Approach to Predict the Glass-Water Reaction." *Nuclear Technology* **176** (1):22–39.

Pierce EM, S Kerisit, EJ Krogstad, SD Burton, BN Bjornstad, VL Freedman, KJ Cantrell, MMV Snyder, JV Crum, and JH Westsik. 2013. *Integrated Disposal Facility FY2012 Glass Testing Summary Report*. PNNL-21812, Pacific Northwest National Laboratory, Richland, Washington.

Pierce EM, P Frugier, LJ Criscenti, KD Kwon, and SN Kerisit. 2014. "Modeling Interfacial Glass-water Reactions: Recent Advances and Current Limitations." *International Journal of Applied Glass Science* **5**(4):421-435. doi:10.1111/ijag.12077.

Rawlins JA, RA Karnesky, R Khaleel, FM Mann, BP McGrail, WJ McMahon, MG Piepho, PD Rittmann, and F Schmittroth. 1994. *Impacts of Disposal System Design Options on Low-Level Glass Waste Disposal System Performance*. WHC-EP-0810, Rev. 0, Westinghouse Hanford Company, Richland, Washington.

Ribet S and S Gin. 2004. "Role of Neoformed Phases on the Mechanisms Controlling the Resumption of Son68 Glass Alteration in Alkaline Media." *Journal of Nuclear Materials* 324:152-64.

Rockhold ML, ZF Zhang, PD Meyer, and JM Thomle. 2015. *Physical Hydraulic, and Transport Properties of Sediments and Engineered Materials Associated with Hanford Immobilized Low-Activity Waste*. PNNL-23711, Pacific Northwest National Laboratory, Richland, Washington.

Sterpenich J and G Libourel. 2006. "Water Diffusion in Silicate Glasses under Natural Weathering Conditions: Evidence from Buried Medieval Stained Glasses." *Journal of Non-Crystalline Solids* **352**:5446-5451.

Vienna JD, A Jiřička, PR Hrma, DK Smith, TH Lorier, RL Schulz, and IA Reamer. 2001. *Hanford Immobilized LAW Product Acceptance Testing: Tanks Focus Area Results*. PNNL-13744, Pacific Northwest National Laboratory, Richland, Washington.

Vienna JD, JV Ryan, S Gin, and Y Inagaki. 2013a. "Current Understanding and Remaining Challenges in Modeling Long-Term Degradation of Borosilicate Nuclear Waste Glasses." *International Journal of Applied Glass Science* **4** (4):283−294. doi:10.1111/ijag.12050.

Vienna JD, DS Kim, DC Skorski, and J Matyas. 2013b. *Glass Property Models and Constraints for Estimating the Glass to be Produced at Hanford by Implementing Current Advanced Glass Formuation Efforts*. PNNL-22631, Pacific Northwest National Laboratory, Richland, Washington.

Wagoner JD. 1996. Letter from JD Wagoner to Prospective Offerors, Request for Proposal (RFP) No. DE-WO6-96RL-3308. U.S. Deparment of Energy, Richland, Washington.

Wolery TJ and SA Daveler. 1992. *EQ6, A Computer Program for Reaction Path Modeling of Aqueous Geochemical Systems: Theoretical Manual, User's Guide and Related Documentation*. UCRL MA 110662 PT IV, Lawrence Livermore National Laboratory, Livermore, California.

Wolff-Boenisch D, SR Gislason, EH Oelkers, and CV Putnis. 2004. "The Dissolution Rates of Natural Glasses as a Function of their Composition at pH 4 and 10.6, and Temperatures from 25 to 74 °C." *Geochimica Et Cosmochimica Acta* **68**(23):4843−4858.

Appendix A

Mineral Phases Identified in PCT Glass Samples

Appendix A

Mineral Phases Identified in PCT Glass Samples

Table A.1. Mineral Phases Identified in PCT Glass Samples by XRD (see Papathanassiu et al. 2011)

Sample ID	Phases Identified
A1-AN105R2	analcime – c – $Na(Si_2Al)O_6•H_2O$, gobbinsite – $Na_5(Si_{11}Al_5)O_{32}•11H_2O$
A1C1-1	analcime – c – $Na(Si_2Al)O_6•H_2O$, gobbinsite – $Na_5(Si_{11}Al_5)O_{32}•11H_2O$ hectorite-15a – $Na_{0.2}(Mg,Li)_3Si_4O_{10}(OH)_2·4H_2O$, stevensite – $(Ca,Na)_xMg_{3-x}Si_4O_{10}(OH)_2$
A1C1-2	analcime – c – $Na(Si_2Al)O_6•H_2O$, phillipsite-Na – $Na_4KAl_5Si_{11}O_{32}(H_2O)_{10}$, stevensite – $(Ca,Na)_xMg_{3-x}Si_4O_{10}(OH)_2$
A2-AP101	chabazite – $Ca_2Al_4Si_8O_{24}•12H_2O$, herschelite – $NaAlSi_2O_6•3H_2O$
A88AP101R1	analcime – $Na(AlSi_2O_6)(H_2O)$
A88Si-15	None
C100GCC	analcime – $NaAl(Si_2O_6)H_2O$, stevensite – $(Ca,Na)_xMg_{3-x}Si_4O_{10}(OH)_2$
LAWA44R10	analcime – $Na(AlSi_2O_6)(H_2O)$
LAWA53	analcime – $NaAl(Si_2O_6)H_2O$
LAWA88R1	analcime – $NaAl(Si_2O_6)H_2O$
LAWA126	chabazite – $Ca_{1.96}Al_{3.9}Si_{8.1}O_{24}(H_2O)_{13}$, herschelite – $NaAlSi_2O_6•3H_2O$
LAWB31	None
LAWB32	None
LAWB35	None
LAWB60	saponite-15Å – $Ca_{0.2}Mg_3(SiAl)_4O_{10}(OH)_2•4H_2O$, stevensite – $Ca_{0.2}Mg_{2.9}Si_4O_{10}(OH)_2•4H_2O$
LAWB73	stevensite – $(Ca,Na)_xMg_{3-x}Si_4O_{10}(OH)_2$, swinfordite-13Å - $Ca_{0.1}(Li,Al)_3Si_4O_{10}(OH)_2•2H_2O$
LAWB81	swinfordite-13a - $Ca_{0.1}(Li,Al)_3Si_4O_{10}(OH)_2•2H_2O$
LAWB89	None
LAWB90	foshagite – $Ca_4(SiO_3)_3(OH)_2$
LAWC23	None
LAWC27	None
LAWC31	analcime – $NaAl(Si_2O_6)H_2O$, stevensite – $(Ca,Na)_xMg_{3-x}Si_4O_{10}(OH)_2$
LAWC32	analcime – $NaAl(Si_2O_6)H_2O$, stevensite – $(Ca,Na)_xMg_{3-x}Si_4O_{10}(OH)_2$, swinfordite-13Å - $Ca_{0.1}(Li,Al)_3Si_4O_{10}(OH)_2•2H_2O$
PNLA126CC	analcime – $NaAl(Si_2O_6)H_2O$, chabazite – $Ca_{1.96}Al_{3.9}Si_{8.1}O_{24}(H_2O)_{13}$

Table A.2. Mineral Phases Identified in PCT Glass Samples by SEM/EDS and XRD (see Papathanassiu et al. 2011)

Sample ID	Possible Secondary Mineral Phase Compositions Based on SEM/EDS	Phases Identified by XRD
A1-AN105R2	analcime, saponite, $Fe(OH)_3$, $Zn(OH)_2$, $Zr(OH)_4$,	analcime, gobbinsite
A1C1-1	analcime, saponite, $Fe(OH)_3$, $Zn(OH)_2$, $Zr(OH)_4$	analcime, gobbinsite, hectorite, stevensite
A1C1-2	analcime, saponite, $Fe(OH)_3$, $Zn(OH)_2$	analcime, phillipsite, stevensite
A2-AP101	chabazite, phillipsite	chabazite, herschelite
A88AP101R1	analcime, chabazite, phillipsite, $Fe(OH)_3$, $Zn(OH)_2$, $Zr(OH)_4$,	analcime
A88Si-15	analcime, chabazite, saponite	None
C100GCC	analcime, chabazite, saponite, $Fe(OH)_3$, $Zn(OH)_2$, $Zr(OH)_4$	analcime, stevensite
LAWA44R10	analcime, saponite	analcime
LAWA53	analcime, chabazite, saponite	analcime
LAWA88R1	analcime, chabazite, saponite, $Fe(OH)_3$, $Zn(OH)_2$	analcime
LAWA126	analcime, chabazite, phillipsite, saponite	chabazite, herschelite
LAWB31	None	None
LAWB32	None	None
LAWB35	saponite, $Zr(OH)_4$	None
LAWB60	chabazite, calcium silicate, stevensite, $Zr(OH)_4$	saponite-15Å, stevensite
LAWB73	calcium silicate, stevensite, $Zn(OH)_2$, $Zr(OH)_4$	stevensite, swinfordite-13Å
LAWB81	saponite, $Fe(OH)_3$, $Zn(OH)_2$, $Zr(OH)_4$	swinfordite-13 Å
LAWB89	calcium carbonate	None
LAWB90	calcium carbonate, calcium silicate	foshagite
LAWC23	chabazite, saponite, $Fe(OH)_3$, $Zn(OH)_2$	None
LAWC27	analcime, calcium carbonate, calcium silicate, saponite, stevensite	None
LAWC31	stevensite, $Zn(OH)_2$,	analcime, stevensite
LAWC32	analcime, saponite, stevensite, $Fe(OH)_3$, $Zn(OH)_2$, $Zr(OH)_4$	analcime, stevensite, swinfordite-13Å
PNLA126CC	analcime, chabazite, saponite, $Fe(OH)_3$, $Zr(OH)_4$,	analcime, chabazite

Distribution*

OFFSITE

Oak Ridge National Laboratory
EM Pierce

U.S. Department of Energy
Office of River Protection
AA Kruger
GL Pyles

Washington River Protection Solutions
EE Brown
PA Cavanah
SE Kelly
KP Lee (AREVA)
WG Ramsey
KH Subramanian
DJ Swanberg
LE Thompson

Savannah River National Laboratory
AD Cozzi
GP Flach
KM Fox
CC Herman
CM Jantzen

Vitreous State Laboratory
H Gan
W Kot
I Muller
IL Pegg

Energy Solutions
I Joseph

Intera
R Andrews

ONSITE

Pacific Northwest National Laboratory
DH Bacon
SD Burton
VL Freedman
SN Kerisit
J Neeway
DK Peeler
JV Ryan
RJ Serne
GL Smith
MM Valenta
JD Vienna
JH Westsik, Jr.

*All distribution will be made electronically.

Pacific Northwest
NATIONAL LABORATORY

Proudly Operated by **Battelle** *Since 1965*

U.S. DEPARTMENT OF
ENERGY

902 Battelle Boulevard
P.O. Box 999
Richland, WA 99352
1-888-375-PNNL (7665)

www.pnnl.gov